



## Novel carbon dots with dual Modulatory effects on the bone marrow and spleen as a potential therapeutic candidate for treating spinal cord injury

Junjin Li<sup>a,1</sup>, Hongda Wang<sup>a,1</sup>, Yuanquan Li<sup>a,1</sup>, Chunzhen Wang<sup>b,1</sup>, Haiwen Feng<sup>a</sup>, Yilin Pang<sup>c</sup>, Jie Ren<sup>a</sup>, Chuanhao Li<sup>a</sup>, Erke Gao<sup>d</sup>, Dejing Zhang<sup>d</sup>, Dunxu Hu<sup>d</sup>, Pengtian Zhao<sup>d</sup>, Han Ding<sup>a</sup>, Baoyou Fan<sup>a</sup>, Tao Zhang<sup>e</sup>, Xiaomeng Song<sup>a</sup>, Zhijian Wei<sup>a,c,2,\*\*</sup>, Guangzhi Ning<sup>a,2,\*\*\*</sup>, Yong-Qiang Li<sup>b,2,\*\*\*\*</sup>, Shiqing Feng<sup>a,c,e,2,\*</sup>

<sup>a</sup> Tianjin Key Laboratory of Spine and Spinal Cord, International Science and Technology Cooperation Base of Spinal Cord Injury, Department of Orthopedics, International Chinese Musculoskeletal Research Society Collaborating Center for Spinal Cord Injury, Tianjin Medical University General Hospital, Tianjin, 300070, China

<sup>b</sup> Institute of Advanced Interdisciplinary Science, School of Physics, Shandong University, Jinan, 250100, China

<sup>c</sup> Orthopedic Research Center of Shandong University and Department of Orthopedics, Qilu Hospital of Shandong University, Cheeloo College of Medicine, Shandong University, Jinan, 250012, China

<sup>d</sup> The First Central Clinical School, Tianjin Medical University, Tianjin, 300070, China

<sup>e</sup> Department of Orthopaedics, The Second Hospital of Shandong University, No. 247 Beiyuan Street, Tianqiao District, Jinan, 250033, China

### ARTICLE INFO

#### Keywords:

Spinal cord injury  
Carbon dots  
Hematopoietic stem cells  
Bone marrow  
Spleen

### ABSTRACT

Spinal cord injury triggers leukocyte mobilization from the peripheral circulation to the injury site, exacerbating spinal cord damage. Simultaneously, bone marrow hematopoietic stem cells (HSCs) and splenic leukocytes rapidly mobilize to replenish the depleted peripheral blood leukocyte pool. However, current treatments for spinal cord injuries overlook interventions targeting peripheral immune organs and tissues, highlighting the need to develop novel drugs capable of effectively regulating peripheral immunity and treating spinal cord injuries. In this study, we designed, synthesized, and characterized novel Ejiao carbon dots (EJCDs) that inhibit myeloid cell proliferation and peripheral migration by promoting HSC self-renewal, and distinct differentiation into erythroid progenitors in vitro and in vivo. Additionally, EJCDs attenuate the immune response in the spleen, leukocytes' reservoir, following spinal cord injury by diminishing the local infiltration of monocytes and macrophages while promoting motor function recovery. These effects are mediated through the downregulation of CCAAT enhancer binding protein- $\beta$  expression in the spleen and the upregulation of FZD4 protein expression in Lin<sup>-</sup> Sca-1<sup>+</sup> c-kit<sup>+</sup> cells (LSKs) within the bone marrow. Our findings demonstrate that EJCDs effectively reduce myeloid cell infiltration post-spinal cord injury and promote neurological recovery, making them promising therapeutic candidates for treating spinal cord injuries.

\* Corresponding author. Tianjin Key Laboratory of Spine and Spinal Cord, International Science and Technology Cooperation Base of Spinal Cord Injury, Department of Orthopedics, International Chinese Musculoskeletal Research Society Collaborating Center for Spinal Cord Injury, Tianjin Medical University General Hospital, Tianjin, 300070, China.

\*\* Corresponding author. Tianjin Key Laboratory of Spine and Spinal Cord, International Science and Technology Cooperation Base of Spinal Cord Injury, Department of Orthopedics, International Chinese Musculoskeletal Research Society Collaborating Center for Spinal Cord Injury, Tianjin Medical University General Hospital, Tianjin, 300070, China.

\*\*\* Corresponding author. Tianjin Key Laboratory of Spine and Spinal Cord, International Science and Technology Cooperation Base of Spinal Cord Injury, Department of Orthopedics, International Chinese Musculoskeletal Research Society Collaborating Center for Spinal Cord Injury, Tianjin Medical University General Hospital, Tianjin, 300070, China.

\*\*\*\* Corresponding author. Institute of Advanced Interdisciplinary Science, School of Physics, Shandong University, Jinan, 250100, China.

E-mail addresses: [weizhijian2002@126.com](mailto:weizhijian2002@126.com) (Z. Wei), [gzning@tmu.edu.cn](mailto:gzning@tmu.edu.cn) (G. Ning), [yqli@sdu.edu.cn](mailto:yqli@sdu.edu.cn) (Y.-Q. Li), [sqfeng@tmu.edu.cn](mailto:sqfeng@tmu.edu.cn) (S. Feng).

<sup>1</sup> Co-first authors.

<sup>2</sup> Co-corresponding authors.

<https://doi.org/10.1016/j.bioactmat.2024.11.032>

Received 10 August 2024; Received in revised form 24 November 2024; Accepted 24 November 2024

2452-199X/© 2024 The Authors. Publishing services by Elsevier B.V. on behalf of KeAi Communications Co. Ltd. This is an open access article under the CC BY-NC-ND license (<http://creativecommons.org/licenses/by-nc-nd/4.0/>).

**Abbreviations**

18F-FDG	18F-fluorodeoxyglucose	GSEA	Gene set enrichment analysis
DPI	Days post injury	H&E	Hematoxylin and eosin
ANOVA	Analysis of variance	HSC	Hematopoietic stem cell
BFU-E	Burst-forming unit-erythroid	IL-10	Interleukin-10
BM	Bone marrow	KEGG	Kyoto Encyclopedia of Genes and Genomes
BMCs	Cells derived from BM	LSK	Lineage-negative Sca-1-positive c-Kit-positive
BrdU	Bromodeoxyuridine	MEP	Megakaryocyte-erythroid progenitor
CCL2	Chemokine ligand-2	MPP	Multipotent progenitor
CEBPB	CCAAT/enhancer-binding-protein- $\beta$	MRI	Magnetic resonance imaging
CFU	Colony-forming unit	PCR	Polymerase chain reaction
CFU-GMEE	CFU that generates myeloid cells	PET-CT	Positron emission tomography-computed tomography
CLP	Common lymphoid progenitor	SCI	Spinal cord injury
CMP	Common myeloid progenitor	SEM	Standard error of the mean
CXCL12	C-X-C motif chemokine ligand-12	SUV	Standardized uptake value
EJCDs	Ejiao carbon dots	TBST	Tris-buffered saline supplemented with tween 20
ELISA	Enzyme linked immunosorbent assay	TEM	Transmission electron microscopy
FTIR	Fourier-transform infrared spectroscopy	TGF	Transforming growth factor
GMP	Granulocyte-macrophage progenitor	TNF	Tumor necrosis factor
		XPS	X-ray photoelectron spectroscopy

**1. Introduction**

Inflammation is a significant factor associated with secondary spinal cord injury (SCI), resulting in localized swelling, impairment of the blood-brain barrier, and decline in neurological function [1,2]. Current therapeutic strategies targeting SCI-related inflammation include hormonal therapy and cytokines, interferons, antibodies, miRNAs, and cell transplantation. These approaches generally focus on specific cell types or cytokines and not on the primary source of inflammatory cells—hematopoietic stem cells (HSCs) [3–7]. SCI-induced disruption of the central nervous fibers creates a dispersed spinal autonomic network resulting in dysregulation of immune functions in the bone marrow (BM) and spleen. This encompasses disparities in the generation of myeloid and lymphoid cells within the BM, dysfunctional immune cell counts and functions in the spleen, excessive leukocyte infiltration, cytotoxicity, and disruption of leukocyte homing post-SCI [8–19]. Therefore, there is an urgent need to target BM HSCs post-SCI to regulate the peripheral immune system, thereby reducing local acute and subacute inflammation and ultimately protecting neurons and promoting motor function recovery.

As the primary cell lineage responsible for producing red and immune cells, HSCs support the regeneration of all blood and immune-related cells [20]. HSCs reportedly play a critical role in central nervous system diseases and immune system disorders [16,21]. The lineage differentiation of HSCs is a strictly regulated process in which a single HSC gradually acquires lineage preferences in multiple directions as it passes through distinct, hierarchically organized progenitor cell populations [22]. This process is influenced by infections, inflammatory stimuli, hormones, and sympathetic nerves and is regulated by factors such as transforming growth factor (TGF)- $\beta$ , chemokine ligand-2 (CCL2), tumor necrosis factor (TNF)- $\alpha$ , C-X-C motif chemokine ligand-12 (CXCL12) [23–25]. Post-SCI, the BM is affected by trauma, stress, neural regulation, and inflammation, leading to dysregulated hematopoiesis, marked by an elevated level of granulocyte-macrophage progenitors (GMP) and excessive infiltration of myeloid cells at the site of injury [16]. The modulations of HSCs by lineage-specific genetic programs to mitigate GMP differentiation bias, diminish myeloid cell generation and infiltration, and thus improve SCI-induced excessive immune responses offers a new and promising therapeutic approach for treating SCI.

Here, we designed and developed Ejiao carbon dots (EJCDs), leveraging the ability of carbon dots (CDs) to enhance the bioavailability of Ejiao (EJs) and retain its biological efficacy in hematopoiesis and its

anti-inflammatory ability while improving its cellular uptake and metabolism, thereby enhancing its anti-inflammatory properties in regulating the systemic immune status post-SCI [26–28]. This study presents a novel dual-functional bio-carbon dot design capable of regulating the BM and spleen, showing promise as a therapeutic agent for SCI.

**2. Materials and methods****2.1. EJCDs synthesis**

To facilitate dissolution, 0.2 g of powdered Ejiao (Dong-E-E-Jiao) was mixed with 10 mL of deionized water and then sonicated for 10 min. Thereafter, the blend was introduced into an autoclave lined with polytetrafluoroethylene and subjected to a temperature of 200 °C for a duration of 12 h in order to induce the reaction. Once the reaction mixture cooled to 25 °C, it underwent high-speed centrifugation and ultrafiltration to remove precursors and macromolecular impurities. This was followed by dialysis to separate the carbon dots from low-molecular-weight contaminants. The samples were then freeze-dried using a vacuum lyophilizer. The solution and freeze-dried powder were both kept at a temperature of 4 °C for future utilization.

**2.2. EJCDs characterization**

A JEM-1011 electron microscope was used to capture transmission electron microscopy (TEM) images. X-ray photoelectron spectroscopy (XPS) measurements were performed using a Thermo Fisher ESCALAB XI + surface analysis system. An X'Pert3 Powder&XRK-900 diffractometer was used to acquire X-ray diffraction patterns. Absorption and fluorescence spectra were measured at room temperature with a U-T6 spectrophotometer and an F970Pro fluorescence spectrophotometer, respectively. Fourier-transform infrared spectroscopy (FTIR) was performed on a Tensor II spectrometer.

**2.3. Mice**

The study was performed on adult female mice aged 4–6 weeks. All mice were housed in a controlled environment free from specific pathogens, with a maximum of five animals per cage. They were subjected to a standard light-dark cycle and provided unrestricted access to water and food. Thorough evaluation was conducted for all procedures

involving animal experimentation, which received official endorsement from the Animal Care and Use Committee of Tianjin Medical University General Hospital (IRB2023-DW-132). This ensured complete adherence to ethical regulations.

#### 2.4. SCI model

A spinal cord contusion model was used to induce SCI. First, mice were anesthetized using isoflurane. Following that, the participants' skin was disinfected and subsequently, a meticulous dissection of the skin, muscles, and fascia took place. This was followed by performing a laminectomy at the T10 vertebra to expose the spinal cord. To induce controlled contusion on the cord, an Impactor Model III was utilized with a 1 mm diameter impactor tip weighing 5 g. The impactor tip was released from a height of 12.5 mm for a duration of 3 s. The muscle, fascia, and skin were sutured in layers. The mice were allowed to recover in their cages, with manual expression of urine performed twice daily, and were allowed to drink water and eat food freely. For mice that were subjected to splenectomy before SCI, the splenic artery and vein were ligated 1 week before the SCI surgery, followed by spleen removal and wound closure.

#### 2.5. Small animal imaging

To assess the spatiotemporal distribution of EJCDs post-intraperitoneal injection, euthanized mice under isoflurane anesthesia were dissected to extract major organs (liver, spleen, lungs, and kidneys), which were then rinsed in ice-cold phosphate buffer saline (PBS) and stored on ice. The IVIS SPECTRUM small animal imaging system was utilized for organ imaging.

#### 2.6. Bone marrow HSC flow cytometry

The BM-derived cells underwent treatment with a red blood cell lysis buffer (BD Biosciences, San Jose, CA, USA). Cell viability was assessed utilizing the Zombie UV™ Fixable Viability Kit (BioLegend, San Diego, CA, USA). Single cells were resuspended in flow cytometry staining buffer for surface antibody staining. Different cell populations were detected through the application of a staining technique on cells derived from BM (BMCs) [21,29].

#### 2.7. Mature Cell flow cytometry staining

For subsequent analyses, the mice from each group underwent euthanasia with isoflurane inhalation, followed by cardiac perfusion in cold PBS. The femur, spleen, and spinal cord were promptly extracted. The spinal cord was completely removed, sliced into 1 mm<sup>3</sup> pieces, and dissociated using the Neural Tissue Dissociation Kit (Miltenyi Biotec, Bergisch Gladbach, Germany). BMCs were flushed with ice-cold PBS, centrifuged, and collected. Pre-euthanasia peripheral blood (200 µl) was collected. Suspended cells were surface-stained with antibodies in buffer, followed by detection using a BD LSRFortessa flow cytometer, and the data were subsequently analyzed with FlowJo V10 software.

#### 2.8. Colony-forming unit (CFU) assays

Cells from the femurs and spleens of mice were extracted in a biosafety cabinet. Cell suspensions were prepared, counted, mixed with MethoCult™ GF M3434 (STEMCELL, Vancouver, BC, Canada) containing growth factors, and placed in a 6-well plate. The colonies were examined after a period of 10 days, utilizing STEMgrid™-6 on an Olympus IX73 microscope. The colonies were identified in accordance with predetermined criteria [30].

#### 2.9. Bromodeoxyuridine (BrdU) assay

The proliferative activity of HSCs was evaluated using BrdU incorporation. BrdU, obtained from MCE (Monmouth Junction, NJ, USA), was dissolved in a solution comprising 15 % dimethyl sulfoxide/PBS and then administered intraperitoneally to the mice at a dosage of 150 mg/kg for a duration of 24 h prior to sacrifice. Subsequently, flow cytometry analysis was conducted by performing intracellular staining for BrdU.

#### 2.10. Enzyme Linked Immunosorbent assay (ELISA)

The BM was rinsed with 1 ml saline, and the supernatant was collected after vigorous centrifugation. Plasma was collected from 200 µl of peripheral blood after resting at 4 °C for 30 min. Norepinephrine levels were quantified using an ELISA kit provided by Eagle Biosciences (New Hampshire, USA).

#### 2.11. Immunofluorescence

Following 3 days of dehydration with a 30 % sucrose solution, extracted spinal cord samples were obtained at optimal cutting temperature and sliced to 10 µm to obtain frozen tissue sections. After blocking, frozen sections were incubated with primary antibodies overnight at a temperature of 4 °C. Subsequently, the sections underwent washing using tris-buffered saline supplemented with tween 20 (TBST) before being fluorescently labeled with secondary antibodies during another overnight incubation at 4 °C. Finally, the sections were mounted using a medium that contains 2,4-diamino phenylindole (Abcam, Cambridge, UK), and captured with a ZEISS A900 microscope. Data were analyzed via ImageJ software.

#### 2.12. Multiplex cytokine assay

BM supernatant and spleen were gathered and preserved at –80 °C until analysis. A 31-plex cytokine and chemokine panel was analyzed using Luminex-based multiplex bead technology. In line with the guidelines provided by the manufacturer, all tests were conducted using a Luminex-100 system (Bio-Rad, Hercules, CA, USA). The collected data was analyzed utilizing Data Pro Manager 1.02.

#### 2.13. Bacterial culture

Peripheral blood was collected from the medial canthus veins of mice, and 100 µL of blood was spread on a ready-to-use Columbia blood agar ready-to-use plate with using a disposable plastic spreader. The plate was then inverted and incubated at 37 °C for 24 h to observe bacterial colony formation.

#### 2.14. Sequencing

The SMART-Seq v4 Ultra Low Input RNA Kit (Clontech) offers a comprehensive approach to preparing low-input RNA libraries. This process started with the conversion of RNA to a cDNA library, followed by a purification step that targets a specific size range of 150–300 base pairs. Adapters were then added to the cDNA using polymerase chain reaction (PCR), preparing the library for sequencing. The library quality was rigorously assessed using an Agilent 2100 Bioanalyzer to check the appropriate size distribution and concentration. Finally, the library was sequenced on an Illumina platform using a 2 × 150 bp paired-end sequencing protocol.

#### 2.15. Real-Time quantitative PCR

The total RNA was isolated from the spleen using TRIzol reagent (Invitrogen, California, USA). Subsequently, first-strand cDNA synthesis SuperMix was utilized for reverse transcription. For PCR amplification,

the Opticon 2 Real-Time PCR detection system (Bio-Rad) was employed.

### 2.16. Catwalk Gait Analysis

Mice scheduled for Catwalk gait analysis (Noldus, Wageningen, Netherlands) underwent acclimatization in a completely dark room. The mouse's footprints on a clean glass runway were captured after each animal's test. Following the test, footprint analysis was performed using the system's software.

### 2.17. Motor-evoked potentials analysis

Motor-evoked potentials were monitored using an evoked potential monitor. Mice were prepared by shaving their head, back, and bilateral limbs, followed by disinfection with povidone-iodine. The motor evoked potentials were recorded according to the manufacturer's guidelines, and reports were generated for subsequent statistical analysis.

### 2.18. Ultrasonography

Mice were anesthetized with isoflurane, and once anesthetized, hair removal cream was applied to their lower abdomen. After cleaning, the mice were fixed on an operating table. Upon starting the high-resolution small animal ultrasound imaging system (Vevo 2100; VisualSonics, Toronto, ON, Canada), a standard probe was applied with ultrasound coupling gel to the abdomen to locate the bladder. Measurements of maximum width, depth, and height were performed in different planes to estimate residual urine volume.

### 2.19. Positron emission Tomography-Computed Tomography (PET-CT)

BM cell activity was assessed with in vivo PET imaging with 18F-fluorodeoxyglucose (18F-FDG) (InliView-3000B) at 3 days post injury (3 DPI). One hour prior to the scanning procedure, an intravenous injection of 200  $\mu$ Ci of 18F-FDG was administered. The mice were then subjected to scanning using a mini-PET-CT scanner (Novel Imaging, Beijing, China) that captured images across an 80 cm  $\times$  80 cm field (160 pixels  $\times$  160 pixels). These images were subsequently reconstructed into three-dimensional projections with dimensions of 336 pixels  $\times$  160 pixels  $\times$  160 pixels. Standardized Uptake Values (SUVs) were measured on CT images of the vertebrae, manubrium, and femur to evaluate the levels of radioactivity.

### 2.20. Magnetic Resonance imaging (MRI)

The images were acquired using a 9.4-T MRI scanner (Bruker) at a time point of 14 DPI. To obtain spinal cord T2-weighted images, we employed a fat-suppression rapid acquisition with relaxation enhancement sequence (repetition time: 1600 ms; echo time: 32 ms; slice thickness: 0.5 mm). The quantification of lesion volumes was conducted using ImageJ software.

### 2.21. Drug administration

The BMCs were treated with FzM1 (MCE) at a concentration of 10  $\mu$ M in combination with EJCDs for an in vitro CFU assay. In the in vivo experiment, a solution of FzM1 was prepared by dissolving it in a mixture of DMSO, PEG300, Tween-80, and saline. The final concentration achieved was 50 mg/kg. Following surgery, mice were treated with a combination of EJCDs and FzM1 through intraperitoneal injection once daily until tissue collection.

### 2.22. Western blot

At 28 days post-SCI, spinal cord tissue was collected, and total protein was extracted using RIPA buffer and quantified by BCA assay. Equal

protein amounts were analyzed by SDS-PAGE, transferred to PVDF membranes, and probed with antibodies against NF200, GFAP, MBP, and GAPDH. Protein bands were detected via ECL and quantified with ImageJ to assess changes in target protein expression.

### 2.23. Antibodies and Primers

Antibodies for the flow cytometric and immunofluorescence analyses used in this study are listed in [Supplementary Tables 1 and 2](#)

### 2.24. Statistical analysis and reproducibility

The statistical software GraphPad Prism (version 9.5.8) was utilized for conducting group comparisons through one-way analysis of variance (ANOVA), two-way ANOVA, and Tukey's post hoc test. Differences between groups were assessed using a two-tailed unpaired *t*-test. The data were presented as the mean  $\pm$  standard error of the mean (SEM). Each experiment was repeated at least three times.

## 3. Results

### 3.1. Preparation, characterization, and biological functions of EJCDs

In this study, we successfully synthesized EJCDs with excellent immunomodulatory effects from donkey-hide gelatin using a hydrothermal method ([Fig. 1](#)). Using TEM, we observed that EJCDs are uniformly dispersed nanoparticles with a quasi-spherical morphology and an average particle diameter of  $2.13 \pm 0.635$  nm, facilitating smooth penetration of biological barriers ([Fig. 2A](#) and [B](#)). High-resolution TEM analysis identified a lattice fringe spacing of 0.21 nm, which coincided with the (100) crystal plane of graphitic carbon ([Fig. 2A](#)). The CDs exhibit high stability in phosphate-buffered saline solution ([Fig. S1](#)). The zeta potential of EJCDs in deionized water, measured using a nanoparticle size and zeta potential analyzer, was  $-17.53 \pm 0.6839$  mV ([Fig. 2C](#)). We employed XPS to identify the elemental components and their chemical states on the surface of EJCDs. The primary elements detected were carbon, nitrogen, and oxygen, with energy peaks at approximately 284.39 eV, 399.24 eV, and 531.04 eV, respectively ([Fig. 2D](#)). The X-ray diffraction pattern of EJCDs exhibited a broad peak at  $2\theta = 22^\circ$ , indicating the amorphous nature of graphitic carbon on its (100) plane ([Fig. 2E](#)). Further examination of the surface components using FTIR revealed a broad absorption band at  $3430\text{ cm}^{-1}$  associated with stretching vibrations of O-H and N-H. Continuous peaks observed at 2940 and  $2872\text{ cm}^{-1}$  were indicative of symmetric and asymmetric stretching vibrations of C-H bonds, respectively. Peaks detected at 1661, 1406, and  $1088\text{ cm}^{-1}$  corresponded to the stretching vibrations of C=C, C-N, and C-O bonds. The FTIR and XPS findings revealed the existence of amino acid-derived functional groups in EJCDs, encompassing amino, carboxyl, hydroxyl, and methyl groups that consist of elements such as C, O, and N. ([Fig. 2F](#)). Photoluminescence is a characteristic feature of CDs that makes them suitable for cell imaging and tracking. Under light excitation, CDs emit light, which facilitates cell labeling for tracking drug distribution to assess therapeutic effects. Three-dimensional fluorescence emission spectra revealed increased emission and excitation wavelengths attributed to the normal size distribution in EJCDs ([Fig. 2G](#)). Ultraviolet-visible absorption spectra revealed two weak absorption bands near 271 nm and 330 nm corresponding to  $\pi$ - $\pi^*$  transitions of conjugated C=C bonds in the carbon core, as well as  $n$ - $\pi^*$  electronic transitions of surface functional groups such as C=O and C=N ([Fig. 2H](#)). The optimal excitation wavelength was 395 nm, with a maximum emission peak of 472 nm ([Fig. 2I](#)).

Stable cellular uptake of drugs is a fundamental prerequisite for therapeutic efficacy [30]. BM, the site of hematopoiesis, houses critical cells, HSCs, and progenitor cells (HSPCs), which are pivotal for producing red blood cells and replenishing peripheral immune cells. Initially, we demonstrated the high biological safety of EJCDs in

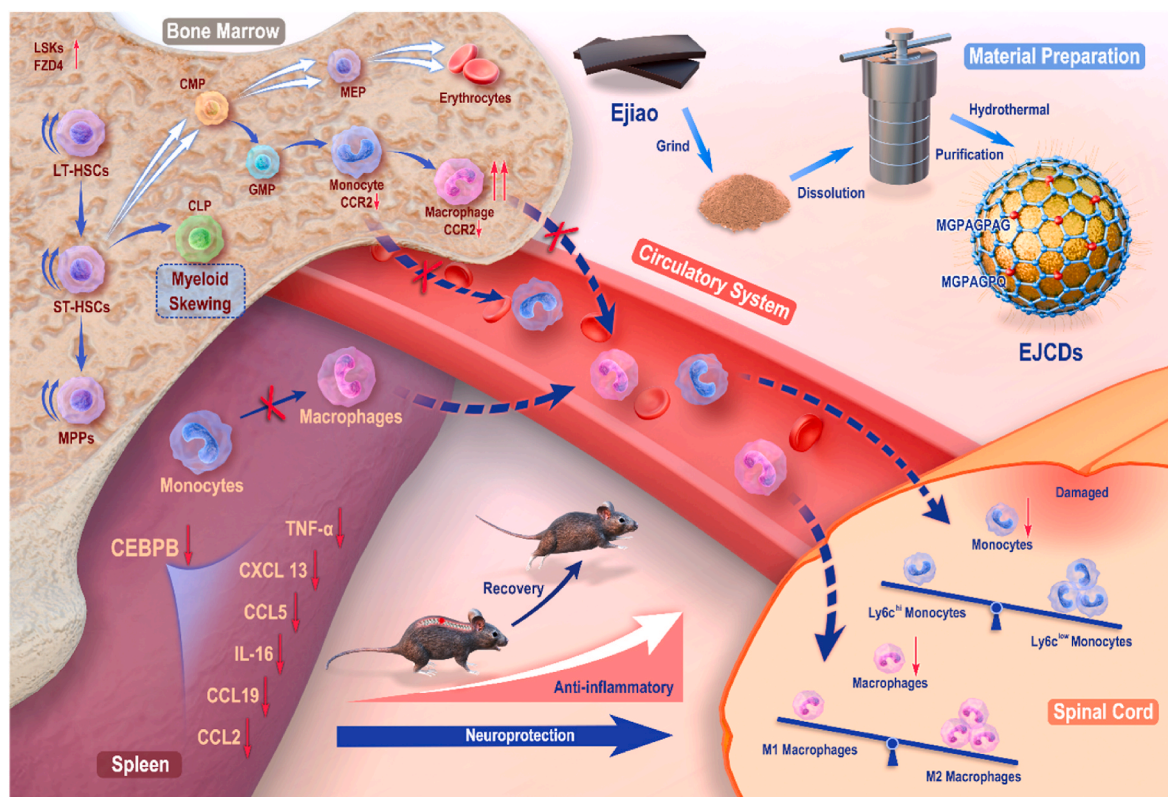


**Fig. 1. Schematic Representation of EJCDs Modulating the Immune System to Repair Spinal Cord Injury in the Bone Marrow and Spleen.** (Material Preparation): EJCDs were obtained from Ejiao through grinding and hydrothermal purification processes. EJCDs were administered intraperitoneally to C57BL/6 mice with spinal cord injuries, where they modulate the immune system to alleviate local inflammatory cells infiltration, reduce inflammation levels, and promote neural repair and motor function recovery in the mice. (Bone Marrow): EJCDs increase the presence of FZD4 on the surface of lineage-negative, Sca-1 positive, c-Kit positive cells and exhibit a strong binding affinity to FZD4 via a specific peptide. This interaction facilitates the self-renewal of HSCs and MPPs, as well as regulating their differentiation trajectory by promoting erythroid differentiation while concurrently reducing myeloid differentiation. This decrease in white blood cells production impedes the migration of macrophages from the BM to the peripheral blood. (Spleen): EJCDs downregulate the expression of CCAAT enhancer binding protein  $\beta$ , decrease the secretion of inflammatory cytokines, reduce the differentiation of monocytes into macrophages, and lessen the migration of mature macrophages to peripheral blood. (Spinal Cord): Due to the dual modulation of the BM and spleen, the infiltration of macrophages and monocytes in peripheral blood decreases, while the proportion of anti-inflammatory macrophages and monocytes increases in the spinal cord, which protects residual neurons and promotes neural function repair.

C57BL/6 mice and their BMCs (Fig. 3A–S2 and S3). In vitro CFU assays of BMCs treated with varying concentrations of EJs and EJCDs demonstrated a positive correlation between the concentration of EJCDs and the formation of burst-forming unit-erythroid (BFU-E) and CFU that generates myeloid cells (CFU-GMEE) colonies, exhibiting significant differences compared with the EJ group (Fig. 3B). The increase in 5-ethynyl-2'-deoxyuridine (EdU)-positive cell counts indicates an increase in BMCs numbers, possibly due to EJCDs-induced proliferation of BMCs (Fig. 3C). To explore the impact of EJCDs on HSCs in vivo, we administered gradient concentrations of EJCDs to mice via intraperitoneal injection. Mouse CFU assays showed a proportional relationship between the concentration of EJCDs (at doses below 50 mg/kg) and the numbers of mouse BM-derived BFU-E and CFU-GMEE colonies. Furthermore, compared with an equivalent dose of EJs, the effects induced by EJCDs were significantly higher, likely due to their enhanced ability to penetrate biological barriers (Fig. 3D).

To investigate the cellular uptake of EJCDs in BMCs in vivo, we used flow cytometry to monitor the uptake of EJCDs in BMCs in vivo. The results showed that Indo-1 violet-A (Filter 450/50) was the optimal channel for detecting EJCDs, with BMCs reaching peak fluorescence within 1 h (Fig. 3E and S4). Given the excellent fluorescence stability of EJCDs, further monitoring of EJCDs distribution was conducted. C57BL/6 mice received an intraperitoneal injection of EJCDs at 50 mg/kg. At various time intervals, the mice were euthanized, and major organs (such as liver, spleen, lungs, and kidneys) were harvested for in vivo

imaging purposes. The results indicated that EJCDs primarily accumulated in the liver and kidneys (Fig. S5). The structural characteristics, small particle size, stability, high bioavailability, exploitation degree, and biological function of BMCs confirmed the potentially significant biological value of EJCDs.

### 3.2. Regulation of HSC proliferation and differentiation by EJCDs

The regeneration of blood cells, including erythrocytes and leukocytes, is a complex process involving the proliferation, differentiation, and migration of HSCs. Previous studies have confirmed that SCI affects hematopoietic function in humans and mice, resulting in post-injury anemia and dysregulation of the immune system [16,31–33]. To investigate the effects of EJCDs on HSC function following spinal cord injury, we established a C57BL/6 wild-type spinal cord contusion mouse model and utilized multi-color flow cytometry to observe these cells in the BM. We observed that after EJCDs administration, there was an increase in both the absolute number of LSK cells and long-term HSCs (LT-HSCs) in the femurs of mice, as well as their proportions relative to Lin<sup>-</sup> cells. The most significant increase occurred on day 3 (Fig. 4A–B and S6). To assess the reasons for changes in HSC numbers, we used BrdU to evaluate the proliferation of LSK cells and LT-HSC populations. Compared with vehicle-injected mice, those injected with EJCDs exhibited significantly enhanced proliferation of LSK cells and LT-HSCs. LSK cells proliferation continued until 14 DPI, whereas LT-HSC

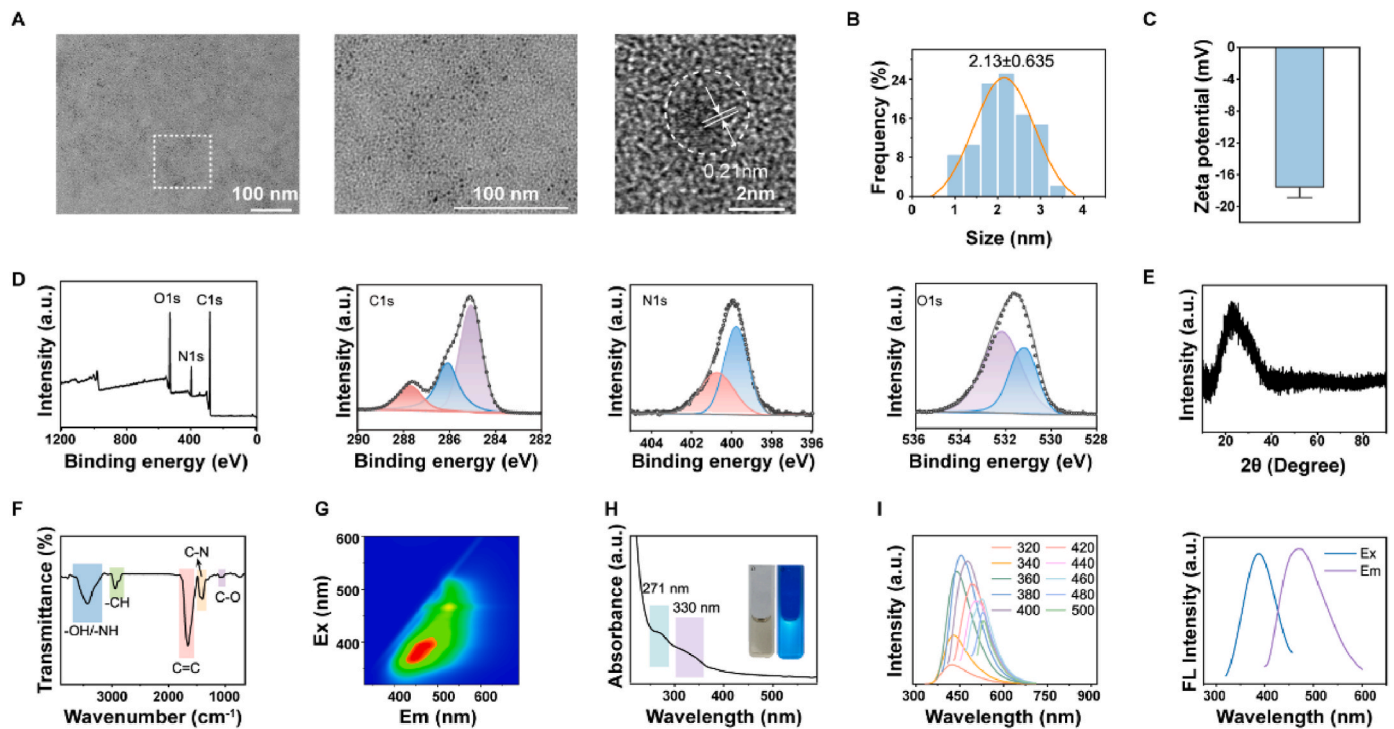


**Fig. 2. Characteristics of EJCDs.** A: TEM and high-resolution TEM images of EJCDs; B: Particle size distribution of EJCDs determined from TEM images; C: Zeta potential of EJCDs in aqueous solution measured using a nanoparticle size and zeta potential analyzer; D: Total X-ray photoelectron spectroscopy (XPS) spectrum, high-resolution C1s spectrum, high-resolution O1s spectrum, and high-resolution N1s spectrum; E: X-ray diffraction (XRD) patterns; F: Fourier-transform infrared spectroscopy (FTIR) spectrum of EJCDs; G: Three-dimensional fluorescence spectra of EJCDs; H–I: Optical properties of EJCDs: ultraviolet–visible absorption spectrum, fluorescence excitation spectrum (blue line), and emission spectrum (purple line).

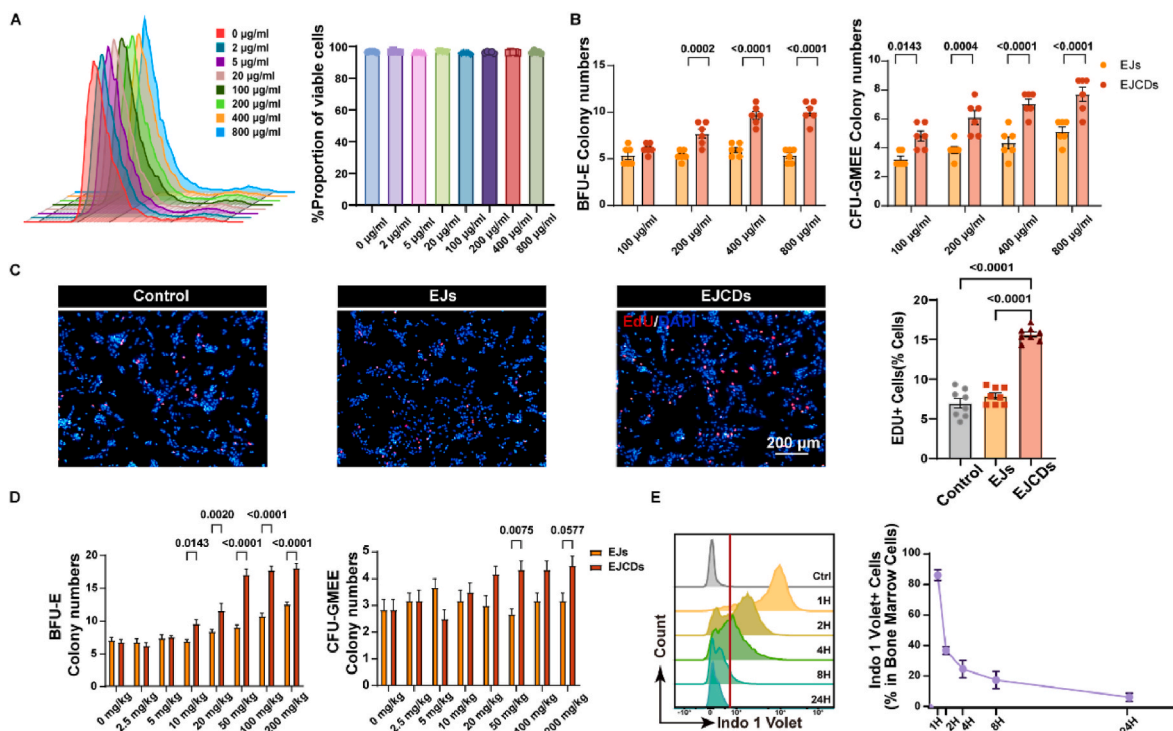


**Fig. 3. Biological Functions of EJCDs.** A: Cell viability and death ratio in mouse BMCs treated with various concentrations of EJCDs for 24 h assessed using live/dead staining. (n = 5); B: Number of BFU-E and CFU-GMEE colonies formed by  $3 \times 10^5$  mouse BMCs cultured for 10 days with various concentrations of EJCDs. (n = 6); C: BMCs treated with 400  $\mu\text{g/ml}$  EJCDs for 24 h, followed by incubation with 10  $\mu\text{M}$  EdU for 24 h. EdU-positive (red) cells and Hoechst 33342-stained nuclei (blue) are detected. The proportion of EdU-positive cells in the BM cell population is measured. (n = 8). Scale bar, 200  $\mu\text{m}$ ; D: Number of BFU-E and CFU-GMEE colonies formed by  $3 \times 10^5$  mouse BMCs extracted from mice 3 days post-intraperitoneal injection of various concentrations of EJCDs and cultured for 10 days. (n = 6); E: Proportion of Indo-1 violet-positive BMCs in mice after intraperitoneal injection of 50 mg/kg EJCDs, analyzed using flow cytometry.

proliferation persisted until 7 DPI (Fig. 4C–F). Employing PET-CT scanning with 18F-FDG in murine subjects, we observed an elevation in 18F-FDG uptake within the vertebrae, femur, and sternum of EJCDs-treated mice compared with vehicle-treated mice, indicating enhanced metabolic activity in BMCs following EJCDs injection (Fig. 4G–H). To further quantify the effects of EJCDs on HSCs in mice post-SCI, Procr-2A-tdTomato mice, expressing red fluorescent protein (tdTomato) exclusively in HSCs and multipotent progenitor cells (MPPs), were used in this experiment. We discovered that on 3 DPI, both the count and BrdU incorporation in HSCs were significantly augmented in the EJCDs-treated Procr-2A-tdTomato mice, consistent with previous findings in the C57BL/6J mice (Fig. 4I–K).

HSCs possess the capability for multilineage differentiation. To provide additional insights into the effects of EJCDs on this diverse populations of cells, both in terms of their physical characteristics and functional consequences, we quantitatively analyzed changes in HSPCs population post-SCI in C57BL/6 mice using flow cytometry. Gating strategies were employed to distinguish separate cellular populations at various time intervals following the injury (Figs. S7 and S8). [21,34]. Compared with the vehicle group, both absolute values and percentage of megakaryocyte-erythroid progenitor (MEP) cells dramatically increased on days 3, 7, and 14 post-injury in the EJCDs group, reaching a peak on 3 DPI (Fig. 4L–M). Conversely, there was a pronounced decrease in absolute values and percentage of myeloid progenitor GMP cells on 3, 7, and 14 DPI compared with those in the vehicle group and Ejs group (Fig. 4N–O and S9). BrdU uptake experiments indicated an enhanced proliferative capacity in common myeloid progenitor (CMP) and MEP cells populations within the EJCDs group, likely attributed to increased numbers and proportions of CMP and MEP, as demonstrated which flow cytometry data (Fig. S10). There was no discernible difference between the vehicle and EJCDs groups regarding common lymphoid progenitor (CLP) cells representing lymphoid progenitors (Fig. S11). MPPs exhibited distinct profiles in differentiation potential and bias [29]. Flow cytometry analysis revealed an increase in MPP2 and MPP3 cell numbers within the EJCDs group, consistent with previous findings (Fig. S12). CFU assays depicted the functionality of HSPCs, including their proliferative capacity and differentiation potential. In BFU-E and CFU-GMME colony formation assays, the EJCDs group exhibited notably enhanced colony-forming ability, with the number and size of colonies markedly increasing, particularly CFU-GMME. This effect was particularly evident from 3 DPI to 7 DPI, indicating an acute response of EJCDs in regulating hematopoiesis after SCI (Fig. S13). Peripheral blood counts in mice indicated that EJCDs, exhibited enhanced erythropoietic activity compared with EJ and the vehicle group (Fig. S14). Simultaneously, the use of EJCDs did not significantly increase the susceptibility of mice to pathogens (Fig. S15). Coagulation function tests demonstrate that EJCDs do not impair the coagulation ability of mice, eliminating the risk of EJCDs-induced postoperative bleeding and thrombosis in mice (Fig. S16).

### 3.3. Effect of EJCDs on bone marrow myeloid Cell production and migration

Because of the short lifespan of monocytes post-SCI, the peripheral blood monocyte level is quickly depleted, mobilizing hematopoietic cells to maintain dynamic equilibrium within the body [35,36]. We analyzed the number and proportion of mature myeloid cells in the BM of C57BL/6 mice post-SCI, comparing the EJCDs-treated group with the vehicle control group. Utilizing high-throughput flow cytometry, it was observed that the EJCDs-treated group exhibited a decrease in monocyte count within the BM after SCI, while no significant variation was found in neutrophil count. These findings are consistent with previous outcomes. (Fig. 5A–B and S17). The percentage and number of macrophages in the BM increased (Fig. 5C). Given the decrease in the number and proportion of monocyte precursors, GMP, and monocytes, we analyzed BrdU incorporation in macrophages to assess their

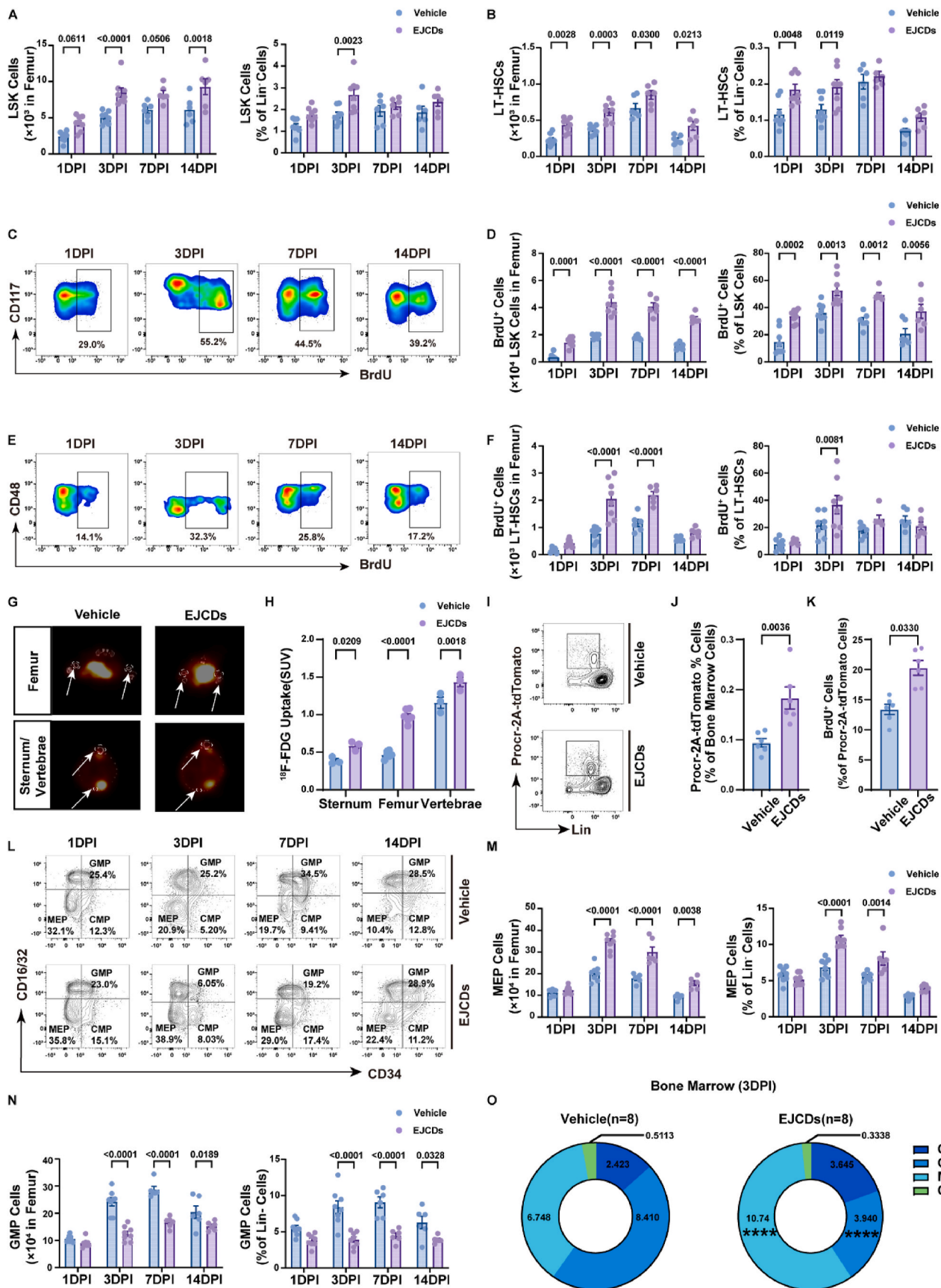
self-proliferation. We found similar BrdU incorporation between macrophages and CD45<sup>+</sup> leukocytes in both vehicle and EJCDs-treated groups (Fig. 5D and E), excluding the possibility that EJCDs promote the proliferation of resident BM macrophages.

To verify whether the increased number of monocytes was associated with reduced migratory capacity, we examined the ratio of monocytes and macrophages in the peripheral blood at similar time points and compared it with that in the BM. There was a proportional relationship between cells in the peripheral blood and those in the BM. These proportional relationships are crucial for clinicians in diagnosing, treating, and monitoring hematological diseases [37–39]. The results showed an evident decrease in the proportion of peripheral blood macrophages within 3–7 DPI in the EJCDs-treated group. However, changes to monocytes were minimal (Fig. 5F–I). These results suggest that EJCDs may restrict the migration of macrophages from the BM. We assessed CCR2 expression in monocytes and macrophages in the BM. The proportion of CCR2-positive macrophages decreased in the EJCDs-treated group, explaining the main reason for the accumulation of macrophages in the BM (Fig. 5J). We conducted an examination of the biological functions of monocytes and macrophages in the BM after undergoing EJCDs treatment. Utilizing high-throughput flow cytometry analysis, we observed a rise in the expression levels of CD169<sup>+</sup> ARG1<sup>+</sup> within this particular subset of macrophages (Fig. 5K). This macrophage subtype contributes to the maintenance of HSCs in the BM [40,41]. Furthermore, we analyzed the expression of Ly6C in monocytes and observed a considerable rise in Ly6C<sup>hi</sup> monocytes in the BM of the EJCDs-treated group post-SCI (Fig. 5L). These cells, typically associated with acute inflammatory responses, are more likely to migrate to inflamed tissues and differentiate into macrophages or dendritic cells, which participate in immune responses and offer protection against neural injury [42]. These findings revealed that EJCDs exhibit noteworthy potential for regulating peripheral immune homeostasis post-SCI by inhibiting the outward migration of macrophages from the BM.

### 3.4. EJCDs inhibit local inflammatory responses after SCI and promote motor function recovery in mice

Considering the significant reduction in leukocytes and monocytes in the bloodstream of mice administered with EJCDs, we hypothesized that cell infiltration at the site of SCI would also be mitigated [35,43,44]. We employed high-throughput flow cytometry to examine different cell subpopulations in the spinal cord during the initial, subsequent, and transitional stages of the immune response following SCI, specifically on days 1, 3, and 14. The findings demonstrated that the EJCDs group exhibited a significantly reduced number of infiltrating white blood cells compared with the control group at various stages of the injury (Fig. S18). To eliminate the impact of spleen-resident monocytes and macrophages on the experimental results, we performed splenectomy on C57BL/6 mice 1 week before inducing SCI, followed by EJCDs treatment. The control group underwent splenectomy and received vehicle treatment (Fig. 6A). EJCDs reduce the proportion of monocytes and macrophages in the spinal cord at 3 DPI and 7 DPI, regardless of whether a splenectomy was performed (Fig. 6B and S19–20). Further analysis of the relationship between monocytes and macrophages revealed increased Ly6C<sup>low</sup> monocytes in the spinal cord of EJCDs-treated mice. These non-classical patrolling monocytes express immunoregulatory cytokines, notably CD206 and interleukin-10 (IL-10) [45]. These cells voluntarily survey the vascular endothelium during inflammation and quickly return to the injury site; however, the number of Ly6C<sup>hi</sup> monocytes decreased (Fig. 6C and D). Similarly, IL10-positive cells in the spinal cord increased following SCI (Fig. 6E). As the differentiation of monocytes into macrophages occurred, there was a notable increase in the population of CD206<sup>+</sup> macrophages, while a significant decrease was observed in the number of CD86<sup>+</sup> macrophages within the spinal cord of C57BL/6 mice treated with EJCDs. (Fig. 6F and G).

Immunofluorescence staining revealed that EJCDs substantially



(caption on next page)

**Fig. 4. EJCDs Promote the Proliferation of HSCs and Regulate their Lineage Differentiation After SCI.** A–B: Impact of EJCDs treatment at various time points post-SCI on hematopoietic progenitor cell numbers. A: Frequency and absolute numbers LSK cells of within the Lin<sup>-</sup> cells determined (1 DPI and 3 DPI: n = 8; 7 DPI and 14 DPI: n = 6); B: Frequency and absolute numbers of LT-HSC within Lin<sup>-</sup> cells measured (1 DPI and 3 DPI: n = 8; 7 DPI and 14 DPI: n = 6); C–F: Effects of EJCDs administration at various time points post-SCI on HSC proliferation. C: BrdU incorporation in LSK cells at different time points; D: Frequency and absolute numbers of BrdU-positive LSK cells (1 DPI and 3 DPI: n = 8; 7 DPI and 14 DPI: n = 6); E: BrdU incorporation in LT-HSC cells at different time points; F: Frequency and absolute numbers of BrdU-positive LT-HSC cells (1 DPI and 3 DPI: n = 8; 7 DPI and 14 DPI: n = 6); G–H: 18F-FDG-PET/CT imaging to assess BM metabolism. G: PET-CT Imaging of Mice. H, Uptake of 18F-FDG in the sternum, femur, and vertebrae (n = 3); I–K: Procr-2A-tdTomato mouse model of SCI, where tdTomato expression is restricted to HSCs and MPPs. I: Flow cytometry image showing tdTomato<sup>+</sup> BMCs on 3 DPI. J: Bar graph displaying the frequency of tdTomato<sup>+</sup> BMCs. K: Bar graph showing BrdU incorporation in tdTomato<sup>+</sup> BMCs (n = 6); L–O: Effects of EJCDs administration at different time points post-SCI on HSC lineage changes. L: MEP, GMP, and CMP at different time points; M: Proportions of MEP, GMP, and CMP on 3 DPI. N: Absolute number and frequency of GMP at different times; O: Absolute number and frequency of MEP at different times (1 DPI and 3 DPI: n = 8; 7 DPI and 14 DPI: n = 6). \*\*\*\*p < 0.0001.

reduced the infiltration of INOS<sup>+</sup> CD68<sup>+</sup> myeloid cells and increased the proportion of ARG1<sup>+</sup> and CD68<sup>+</sup> myeloid cells (Fig. S21). Additionally, Catwalk gait analysis showed that EJCDs-treated mice exhibited enhanced motor function in the hind limbs, reduced overuse of forelimbs, and enhanced gait regularity post-SCI, contributing to the recovery of locomotor function (Fig. 6H and S22). Electrophysiological testing of the spinal cord's internal electrical signal conduction suggested that the latency of the action potential was reduced and the amplitude increased in the EJCDs group compared to the vehicle group, indicating that EJCDs enhance the conduction of motor electrical signals after SCI (Fig. 6I). In addition, the therapeutic effects of EJCDs on SCI manifested in the recovery of urinary function and a reduction in the magnitude of the injury in the epicenter (Fig. S23). These findings revealed that EJCDs conspicuously regulate the peripheral immune system, reduce inflammatory responses in injury sites, and promote the recovery of motor functions.

### 3.5. EJCDs suppress splenic immune Cell Output after SCI

The spleen serves two important functions, acting as a filter for red blood cells and playing a vital part in the functioning of the immune system. Furthermore, it contains a diverse array of immune cells that play crucial roles in both typical and atypical physiological circumstances [46–48]. We investigated the immune relationship between the spleens of mice treated with EJCDs and those treated with vehicle control. Gross examination revealed no significant difference in the spleen weight; however, the spleen/body weight ratio was lower in mice treated with EJCDs than in mice treated with the vehicle (Fig. 7A). Under certain pathological conditions, HSCs can migrate from the BM to extramedullary organs for extramedullary hematopoiesis [49]. Flow cytometric analysis showed no significant differences in LSK cells and HSCs in the spleens and peripheral blood of EJCDs-treated mice and vehicle-treated mice (Fig. S24). Hematoxylin and eosin (H&E) staining showed an enlarged red pulp region in the spleens of mice treated with EJCDs, possibly due to a rise in the erythrocyte ratio (Fig. 7B). Flow cytometric analysis of immune cell numbers and proportions within the spleen at different time points showed a reduction in myeloid cell numbers in the EJCDs group, with no significant changes in lymphocytes (Fig. 7C and S25).

High-throughput nanostring transcriptome screening and multiplex protein sequencing were used to determine the molecular characteristics of splenic cells exposed to EJCDs to explore the effect of EJCDs on the spleen at genetic and protein levels in mice post-SCI. Mice were sacrificed on 3 DPI to extract the spleen when the peak difference in peripheral immune levels occurred. The principal component analysis results revealed reproducibility among three biological replicates. They highlighted the differences between the groups (Fig. 7D), showing that the spleens exposed to EJCDs had unique expression characteristics. An unbiased analysis of the splenic cell transcriptome revealed that, compared with that in the controls, 855 transcripts were upregulated, and 2051 transcripts were downregulated in the EJCDs group. Gene set enrichment analysis (GSEA) revealed major changes in genes involved in the immune response pathways (Fig. 7F and S26). The GSEA findings revealed that, in comparison to the control group, there was a notable

decrease in the expression of various immune-related pathways within the spleen among individuals receiving treatment. This suggests that the therapeutic intervention may exert inhibitory effects on immune functions specifically localized in the spleen (Fig. 7G). In the spleens of EJCDs-treated mice, CEBPB was significantly suppressed, as confirmed by RT-PCR, indicating that EJCDs achieve immunoregulation by inhibiting the maturation and functionalization of monocytes (Fig. 7H). Multiplex assays analyzing cytokine levels in splenic cells showed reductions in key monocyte chemotactic and inflammatory factors, including CCL5, CCL19, CCL20, IL-16, and TNF- $\alpha$  (Fig. 7I and S27). Overall, these data illustrate that EJCDs reduce inflammatory responses at the injury site by suppressing the mobilization of myeloid cells within the spleen.

### 3.6. EJCDs modulate HSCs proliferation and differentiation through the FZD4-Wnt pathway to repair SCI

The activity of HSCs is regulated through a coordinated interplay of extrinsic and intrinsic signals [50]. To investigate the molecular differences in BM HSCs induced by EJCDs, ELISA results showed a decrease in serum norepinephrine concentrations on 3 DPI in EJCDs-treated mice (Fig. S28). In the BM supernatant of mice treated with EJCDs, multiplex analysis revealed notable increases in CCL19 and CXCL12 and reductions in CXCL11 and IL-2 (Fig. S29). LSK cells were isolated from the femurs of mice on 3 DPI, coinciding with the peak of LSK cells activity. The principal component analysis demonstrated reproducibility among three biological replicates. It highlighted the differences between groups (Fig. 8A), indicating unique expression characteristics in the femoral LSK cells population exposed to EJCDs. Unbiased analysis of the LSK cells transcriptome indicated that there was an increase in 768 transcripts and a decrease in 2031 transcripts following EJCDs treatment in mice, as compared to the control group (Fig. 8B). According to the Kyoto Encyclopedia of Genes and Genomes (KEGG) enrichment analysis results, these genes indicated significant impacts on HSC lineage, porphyrin metabolism, and cytokine–cytokine receptor interaction (Fig. 8C).

Additionally, in LSK cells derived from SCI mice, there was a notable upregulation of FZD4 (Fig. 7D), a critical component of the Wnt signaling pathway, serving a crucial function in cell proliferation, differentiation, and development [51–53]. Flow cytometry also showed an increase in FZD4 expression in LSK cells collected at 3 DPI treatment with EJCDs (Fig. 8E). Prior research has established the involvement of FZD4 in HSC development [54–57]. We then used an effective FZD4 antagonist, FzM1, to block its activity in HSCs both in vitro and in vivo. CFU assays revealed that FzM1 reduced the number and clone size of BFU in vitro and in vivo (Figs. S30 and S31). In C57BL/6 mice post-SCI, FzM1 eliminated the increase in HSCs numbers and their proliferation in the BM induced by EJCDs (Fig. 8F and S32), altered the immune cell homeostasis in the BM and peripheral blood (Fig. 8G–S33 and S34), and increased the numbers of myeloid progenitors and Ly6C<sup>low</sup> monocytes (Fig. 8H). Moreover, FzM1 reduced the infiltration of Ly6C<sup>low</sup> monocytes at the injury site, but had no significant effect on the polarization phenotype of the infiltrating macrophages (Fig. 8I–J and S35). FzM1 induced local immune state changes that led to worse motor function

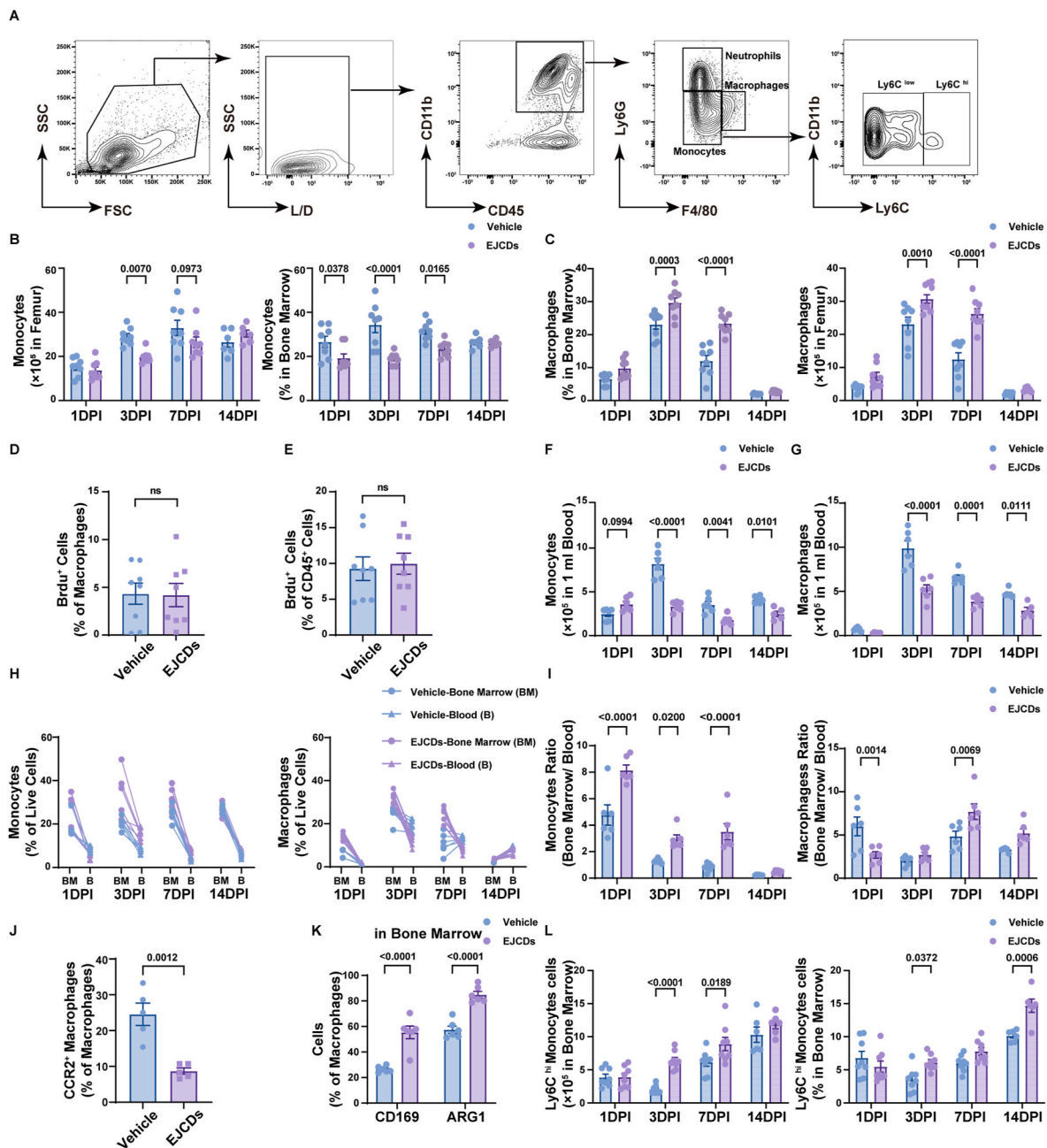


**Fig. 5. EJCDS Regulate Bone Marrow Microenvironment Homeostasis.** A: Flow cytometry plots showing gating strategies for BM monocytes, macrophages, neutrophils, Ly6C<sup>low</sup> monocytes, and Ly6C<sup>hi</sup> monocytes; B–C: Effects of EJCDS administration at different time points post-SCI on myeloid cell numbers in the BM. B: Frequency and absolute numbers of monocytes determined (1 DPI, 3 DPI and 7 DPI: n = 8; 14 DPI: n = 6); C: Frequency and absolute numbers of macrophages determined (1 DPI, 3 DPI and 7 DPI: n = 8; 14 DPI: n = 6); D–E: Proliferation of myeloid cells on 3 DPI in the experimental and control groups. D: BrdU incorporation in macrophages measured (n = 8); E: BrdU incorporation in CD45<sup>+</sup> cells measured (n = 8); F–I: The experimental and control groups after SCI at a specific time point: the absolute number of white blood cells in the peripheral blood (n = 6); H–I: The number of leukocytes in the BM/peripheral blood at specific time points after spinal cord injury in the EJCDS and vehicle groups (n = 6); J: Expression of CCR2 in macrophages in the BM on 3 DPI in the experimental and control groups (n = 5); K: Expression of CD169 and ARG1 in macrophages in the BM on 3 DPI in the experimental and control groups (n = 6); L: The frequency and total count of Ly6Chi mononuclear cells in the BM at various time intervals following spinal cord injury (1 DPI, 3 DPI and 7 DPI: n = 8; 14 DPI: n = 6).

recovery and spinal cord electrophysiological capacity in mice, compared to EJCDS (Fig. 8K–L and S36–37). Western blot results showed that FzM1 increased glial scar formation (GFAP) while reducing the expression of neurofilaments (NF200) and myelin proteins (MBP) (Fig. S38). We identified the two peptides, MGPAGPQ and MGPAGPAG, with the highest EJCDS content using LC-MS/MS analysis. Subsequently, employing AutoDock Vina software, we computationally determined that these two peptides exhibit a robust binding affinity to FZD4 on the

cellular membrane (Fig. 8M). The results showed that post-SCI in mice, EJCDS enhance HSC proliferation through the FZD4–Wnt pathway, promoting differentiation towards the MEP lineage while reducing the mobilization of monocytes and macrophages in the BM. This reduction in local immune cell infiltration and early inflammatory response subsequently improves motor function recovery post-SCI.

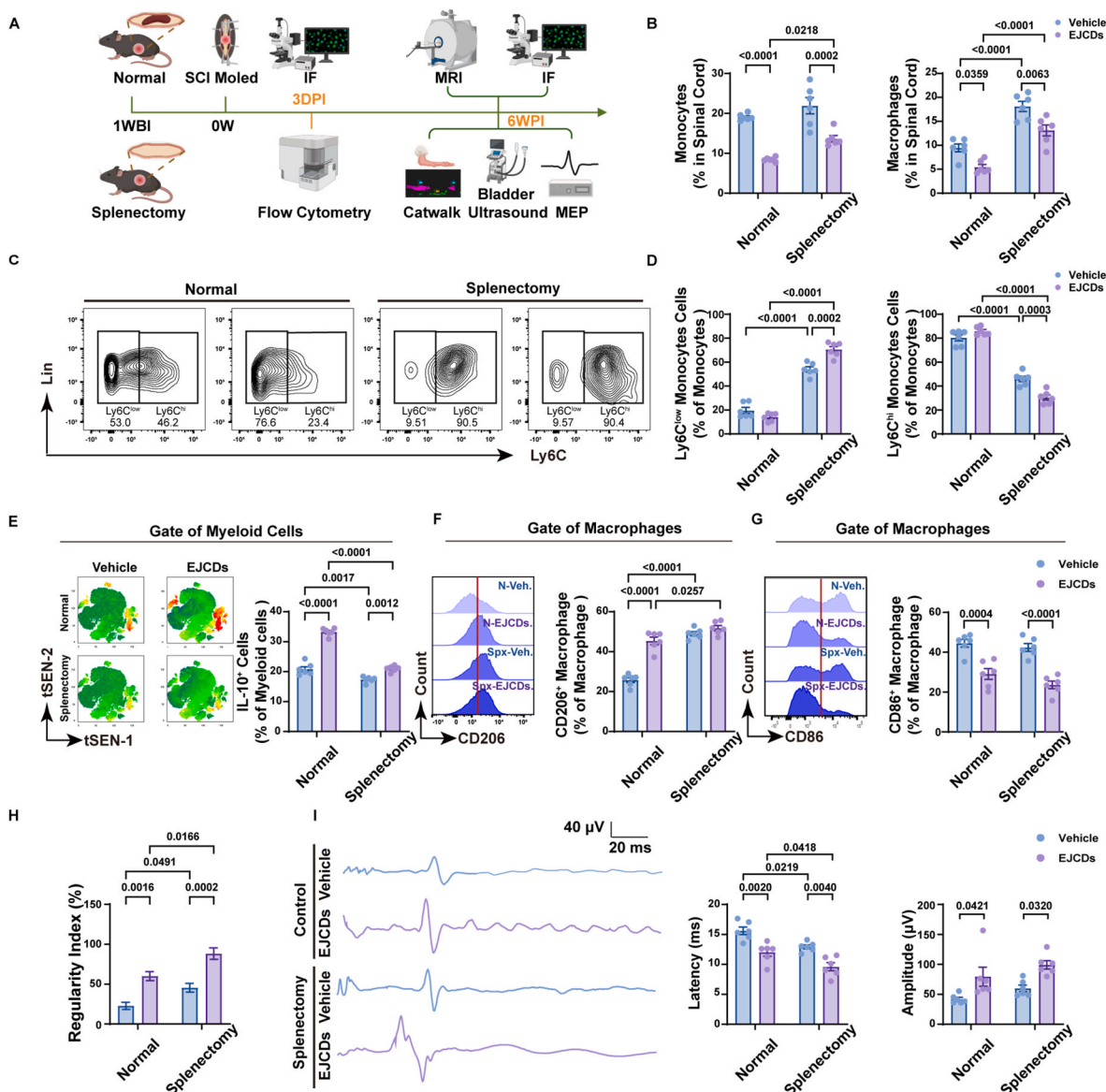


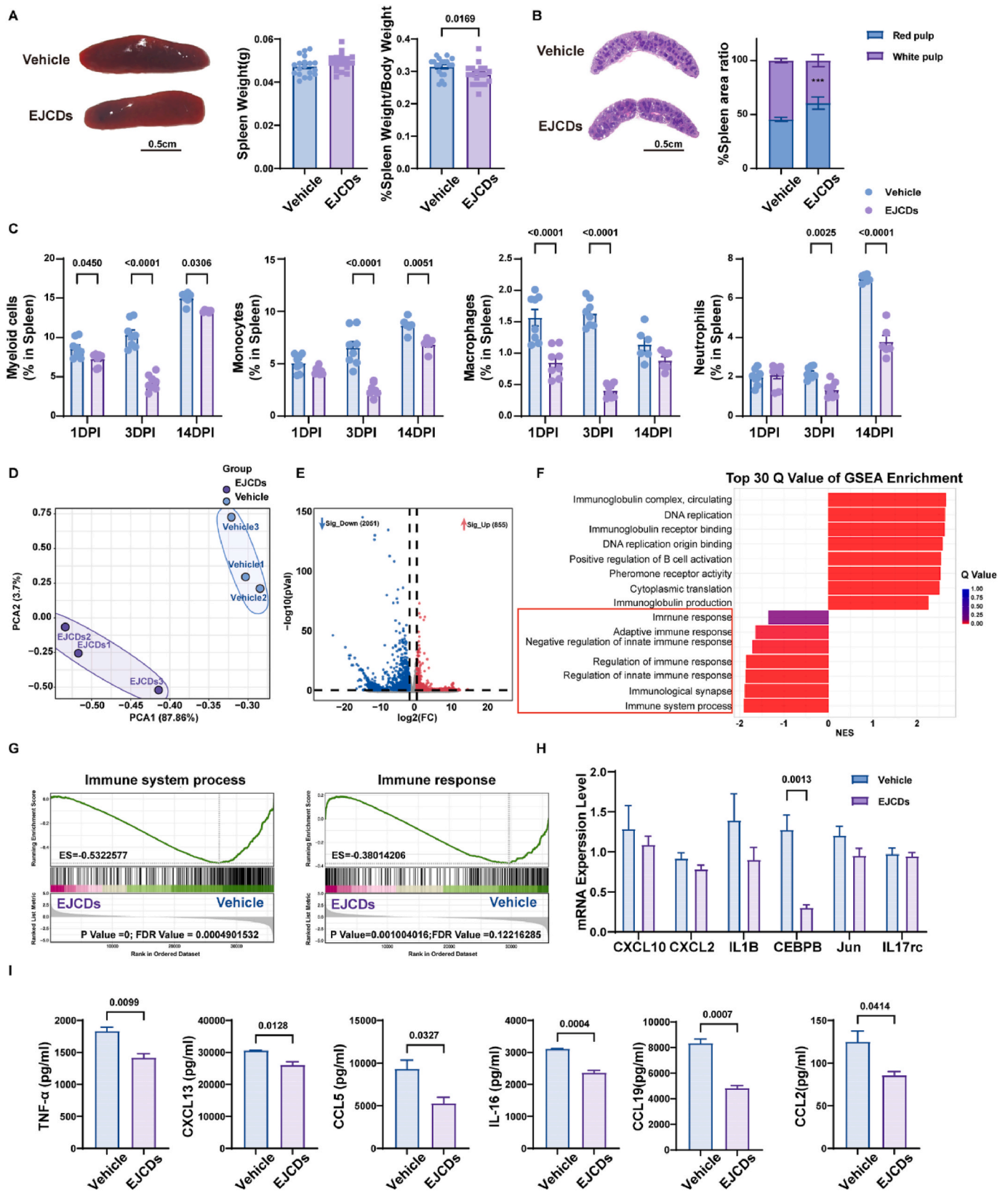
**Fig. 6.** EJCDs Promote Functional Recovery After SCI. A: Schematic illustration of EJCDs-induced functional recovery after SCI; B: Frequency of monocytes and macrophages as a percentage of all live cells in the spinal cord 3 DPI (n = 6); C–D: Frequency of Ly6C<sup>hi</sup> and Ly6C<sup>low</sup> monocytes within all live spinal cord cells on 3 DPI (n = 6); E: Frequency of IL-10<sup>+</sup> cells among all myeloid cells in the spinal cord on 3 DPI (n = 6); F–G: Frequency of CD206<sup>+</sup> and CD86<sup>+</sup> macrophages within all live spinal cord cells on 3 DPI (n = 6); H–I: Assessment of motor function recovery 6 weeks post-SCI, H: Evaluation of hindlimb functional recovery in mice using Catwalk Gait Analysis (n = 6); I: Electrophysiological assessment measuring motor-evoked potential conduction amplitude and latency in the spinal cord (n = 6). Fig. 6A created in BioRender. Hongda Wang (2024). <https://BioRender.com/z78z546>.

#### 4. Discussion

In this study, we developed a novel and promising therapy for SCI that targets immune dysregulation in the spleen and BM, unlike conventional treatments that primarily focus on alleviating symptoms at the injury site [58–60]. The BM, which houses the HSCs, stands at the apex of all immune cells in the body while the spleen serves as the principal reservoir for these immune cells. Existing research indicates that post-SCI anomalies in nerve conduction and hormone levels lead to systemic immune system and immune organ dysfunction [15,61]. Imbalances in immune organs result in the excessive activation of inflammatory cells following SCI, exacerbating secondary damage and further impairing neural function. The interplay between neural function impairment and persistent immune cell infiltration creates a vicious cycle, aggravating early motor function deficits post-SCI. Current treatments, such as corticosteroids or cell transplantation, target

inflammatory responses at the injury site but fail to disrupt this cycle [62,63]. Our findings suggest that regulating the primary sources of infiltrating myeloid cells post-SCI, namely the BM and spleen, can significantly enhance recovery.

In recent years, the application of nanotechnology in biomedicine has garnered extensive attention, particularly CDs, due to their preparation process, structure, and physicochemical properties [64,65]. With their small particle size, simple purification techniques, and ease of post-modification, CDs can effectively deliver drugs across the blood-brain barrier to lesion sites, enhancing their efficacy in the central nervous system and hematopoietic cells [66–69]. Previous studies have demonstrated that donkey-hide gelatin, known as EJs, can modulate the immune system by enhancing HSCs proliferation and improving the BM microenvironment [70–72]. However, the practical application of this compound in clinical settings has been constrained due to its limited water solubility and low bioavailability. Our study reveals that by



(caption on next page)

**Fig. 7. EJCDs Suppress Splenic-Origin Immune Responses** A: Observation of macroscopic spleen metrics on 3DPI. Left: Representative gross image of a mouse spleen, scale bar 0.5 cm. Right: Graph illustrating the weight of the spleen and its proportion to overall body weight ( $n = 19$ ); B: Observation of macroscopic spleen metrics on 3DPI. Left: Representative image of mouse spleen slices stained with hematoxylin and eosin, scale bar 0.5 cm. Right: Graph depicting the proportion of red and white pulp in the spleen ( $n = 5$ ); C: Proportions of myeloid cells, monocytes, macrophages, and neutrophils in viable splenic cells of the experimental and control groups at 1 DPI, 3 DPI, and 14 DPI (1 DPI and 3 DPI:  $n = 8$ ; 14 DPI:  $n = 6$ ); D–G: Transcriptomic changes in mouse spleen on 3 DPI: Comparison between spleens from EJCDs-treated and control mice. D: Principal component analysis showing the first and third components of all samples. E: Number of differentially expressed genes in the spleens of EJCDs-treated and control mice, adjusted for multiple hypothesis testing ( $p < 0.05$  and  $|\log_2(\text{fold change})| > 1$ ). F: Results of GSEA Hallmark analysis indicating enriched gene sets. G: Enrichment plot analysis from GSEA Hallmark depicting immune-related pathways in spleen, displaying the profile of the enrichment score as it progresses and indicating the location of members belonging to a gene set in the list that has been ranked ( $n = 3$ , each comprising spleens from five mice); H: Expression results of TNF pathway genes measured using RT-PCR ( $n = 3$ ); I: Expression of chemokines and inflammatory factors in mouse spleen assessed using mouse chemokine assays ( $n = 3$ , each comprising spleens from five mice).

preparing EJCDs from EJ, their ability to promote HSC proliferation and shift differentiation towards erythroid cells is further enhanced. Three days post-SCI, EJCDs significantly reduce the number of inflammatory cells in peripheral blood and at the injury site and lower the spleen's inflammation levels.

The superior performance of EJCDs compared to EJs can be attributed to several factors. First, EJCDs possess hydrophilic functional groups, which significantly enhance their dispersion and stability in aqueous solutions. This improved solubility and uniform distribution in the body allows EJCDs to more effectively enter the bloodstream. Additionally, the nanoscale structure of EJCDs facilitates their passage through complex biological barriers, such as the blood-brain barrier (BBB). Although this study does not directly address the effects of EJCDs on the nervous system, this characteristic of CDs is particularly valuable in the treatment of central nervous system-related disorders. Finally, due to their small particle size and large surface area, EJCDs offer more active sites for interaction with target molecules, enhancing their activity and stability within the body. These structural advantages contribute to the improved therapeutic efficacy of EJCDs over EJs. EJCDs have shown outstanding effects as a novel immunomodulatory drug and in the treatment of SCI. However, their delivery method still needs improvement. Utilizing the hydrophilicity of EJCDs to develop various polymer carriers or hydrogel carriers for their controlled release, and optimizing the dosage and delivery methods, will be the focus of our future research.

HSCs, located at the highest point of both the blood system and immune cells, exhibit two essential characteristics: the ability to regenerate themselves and transform into myeloid and lymphoid cells. Current studies also indicate that BM hematopoiesis plays a role in the onset and repair of degenerative and traumatic diseases of the central nervous system. In the late stages of SCI, the failure of BM HSC function results in a decreased production of mature lymphocytes, increasing the risk of infection and mortality in patients [16]. Our study focused on the early stages of SCI, where myeloid cells extensively infiltrate the injury site. Promoting HSC differentiation towards erythroid cells, reduced the production of myeloid cells. Additionally, our results showed a marked inhibition of myeloid cell migration from the BM, likely due to the downregulation of CCR2 expression, which is crucial for their migration to inflammatory sites. CD169<sup>+</sup> and ARG1<sup>+</sup> macrophages are able to maintain a stable internal environment for HSCs in the BM [40,41], but the function of macrophages in the BM is not well defined.

This study has some limitations. First, while we found that EJCDs have the ability to regulate the proliferation and differentiation of BM HSCs after SCI in mice and promote motor function recovery, EJCDs do not possess BM-targeting capabilities. Therefore, their effects on other tissues and organs, such as the FZD4-Wnt signaling pathway in non-target tissues, remain to be explored. Second, our study identified FZD4 as a molecular switch regulating hematopoietic function in mice, but FZD4 may not be the only critical factor in the interaction between EJCDs and the hematopoietic system in SCI. The roles of other molecules warrant further investigation. Third, the study would benefit from implementing methods to trace the migration of HSCs and their differentiated progeny, such as using Fgd5-CreER/tDTomato mice and two-photon in vivo imaging. Lastly, enhancing the targeting ability of

EJCDs specifically toward HSCs or developing biological carriers for EJCDs delivery could mitigate or eliminate potential off-target effects on other tissues or organs.

The therapeutic effects of EJCDs are likely mediated through their impact on key signaling pathways, such as the FZD4-Wnt pathway, which regulates cells proliferation and lineage determination [73,74]. Our findings demonstrated that modulating FZD4 influences cell fate decisions and ameliorates post-traumatic pathological immune responses. This study expands the understanding of this pathway in SCI recovery and its potential application in other central nervous system diseases. Furthermore, we screened high-affinity peptides within EJCDs for FZD4, providing new insights into the effects of EJCDs on HSCs.

## 5. Conclusion

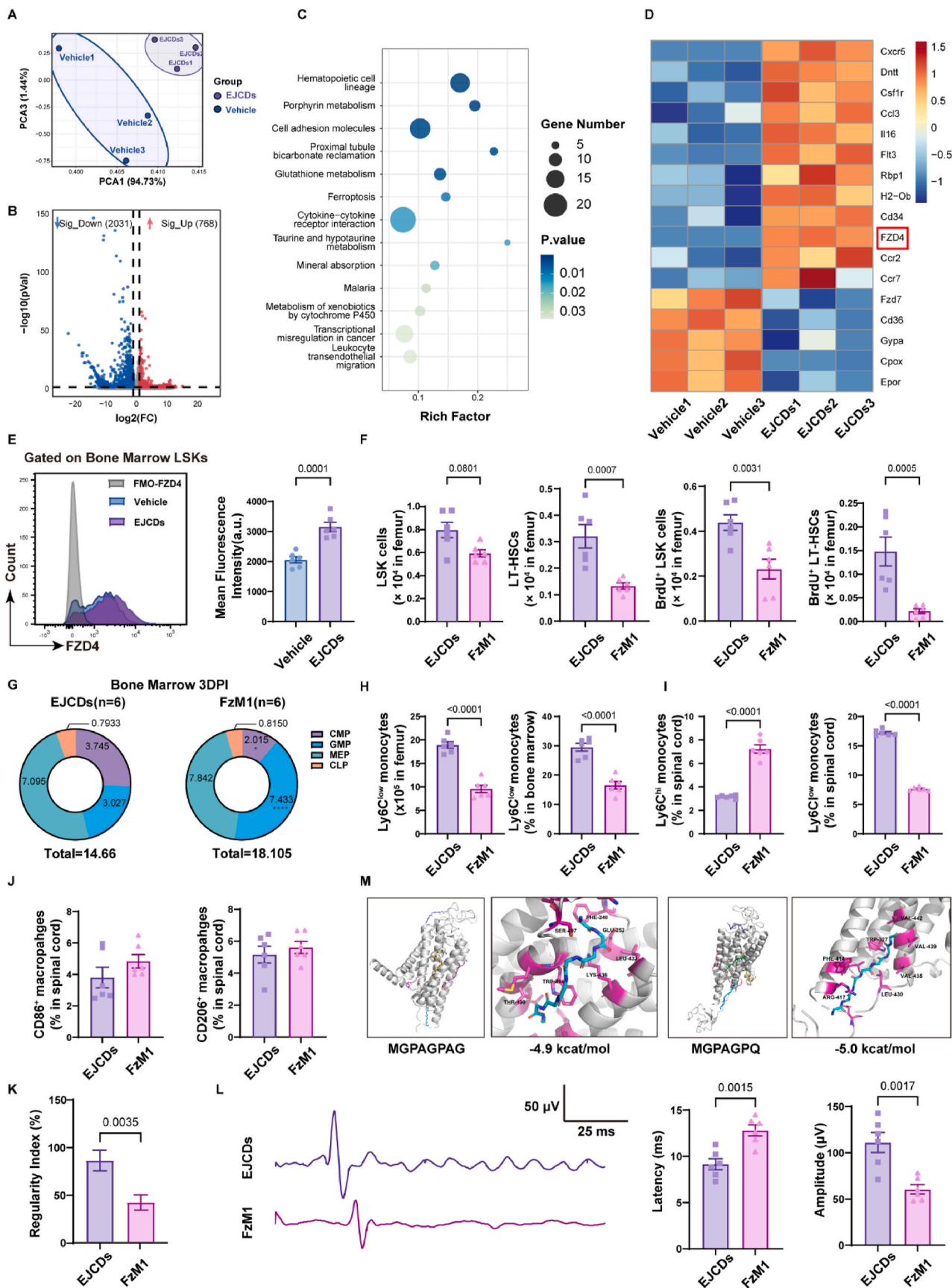
This study revealed that CDs enhance the efficacy of precursor biological treatments, achieving broader therapeutic effects. To this end, immunomodulatory EJCDs were engineered to modulate the disordered hematopoietic system following SCI, regulate HSC lineage differentiation, and thus impact downstream mature immune cells, providing therapeutic benefits. The results revealed that EJCDs can suppress local inflammatory cell infiltration after SCI, alleviate secondary damage, protect residual neurons, and promote neurological function recovery. Due to their inherent nanostructure, the mechanisms underlying these outcomes are multifaceted: 1) EJCDs control the proliferation and differentiation of HSCs in the BM of mice post-SCI via the FZD4-Wnt signaling pathway, influencing the generation and mobilization of new myeloid cells; and 2) EJCDs downregulate the expression of CEBPB in the spleen of mice, reducing the mobilization of splenic myeloid cells and thus attenuating the inflammatory response at the injury site. This strategy of modulating the functional state of systemic immune organs to affect local immune homeostasis at the injury site represents a promising potential therapeutic approach for treating SCI.

## CRedit authorship contribution statement

**Junjin Li:** Visualization, Validation, Software, Methodology, Data curation. **Hongda Wang:** Writing – original draft, Visualization, Methodology. **Yuanquan Li:** Writing – original draft, Methodology. **Chunzhen Wang:** Software, Methodology. **Haiwen Feng:** Methodology. **Yilin Pang:** Methodology. **Jie Ren:** Methodology. **Chuanhao Li:** Software. **Erke Gao:** Methodology. **Dejing Zhang:** Methodology. **Dunxu Hu:** Methodology. **Pengtian Zhao:** Methodology. **Han Ding:** Methodology. **Baoyou Fan:** Methodology, Investigation. **Tao Zhang:** Resources. **Xiaomeng Song:** Methodology, Investigation. **Zhijian Wei:** Software, Methodology. **Guangzhi Ning:** Writing – original draft, Validation, Supervision. **Yong-Qiang Li:** Writing – original draft, Funding acquisition. **Shiqing Feng:** Writing – original draft, Resources, Project administration, Investigation, Funding acquisition.

## Data availability

The data supporting the findings of this study are available on request from the corresponding author. The data are not publicly



(caption on next page)

**Fig. 8. EJCDS Regulate Bone Marrow Microenvironment Homeostasis Through the FZD4-Wnt Signaling Pathway.** A–D: Changes in the transcriptome of LSK cells in the femoral BM of mice on 3 DPI: Comparison between EJCDS-treated LSK cells and control LSK cells. A: Analysis of the first and third components in all samples using principal component analysis.; B: Number of differentially expressed genes between the LSK cells in the EJCDS-treated and control mice, adjusted for multiple hypothesis testing ( $p < 0.05$  and  $|\log_2(\text{fold change})| > 1$ ); C: KEGG pathway enrichment analysis of EJCDS-treated LSK cells; D: Heatmap of genes involved in the proliferation and differentiation of LSK cells ( $n = 3$ , each sample containing femoral BMCs from five mice); E: Analysis of FZD4 protein expression on the membrane of LSK cells ( $n = 6$ ); F: Analysis of the number and proliferation of LSK cells and long-term HSCs in the femoral BM of mice treated with EJCDS and FZM1 ( $n = 6$ ); G: Proportion of MEP, GMP, and CMP in the femoral BM of mice treated with EJCDS and FZM1 on 3 DPI ( $n = 6$ ); H: Analysis of the absolute numbers and proportion of Ly6c<sup>low</sup> cells in the BM on 3 DPI ( $n = 6$ ); I–J: Analysis of myeloid cell subtypes and their proportions in the spinal cord on 3 DPI. I: Proportion of Ly6c<sup>hi</sup> and Ly6c<sup>low</sup> monocytes among live cells in the spinal cord. J: Proportion of CD206<sup>+</sup> and CD86<sup>+</sup> macrophages among live cells in the spinal cord ( $n = 6$ ); K: Whole and close-up views of combined protein peptides MGPAGPQ and MGPAGPAG; L: Evaluation of hindlimb function recovery in mice using Catwalk gait analysis ( $n = 6$ ); M: Electrophysiological assessment measuring motor-evoked potential conduction amplitude and latency in the spinal cord ( $n = 6$ ).

available due to privacy or ethical restrictions.

### Ethics approval and consent to participate

Thorough evaluation was conducted for all procedures involving animal experimentation, which received official endorsement from the Animal Care and Use Committee of Tianjin Medical University General Hospital (IRB2023-DW-132). This ensured complete adherence to ethical regulations.

### Declaration of competing interest

The authors declare that they have no known competing financial interests or personal relationships that could have appeared to influence the work reported in this paper.

### Acknowledgements and funding sources

This work was supported by grants from the National Key Research and Development Project of Stem Cell and Transformation Research (2019YFA0112100), the National Natural Science of China (81930070, 82102671), Tianjin Key Medical Discipline (Specialty) Construct Project (TJYXZDXK-027A), Tianjin Science and Technology Project (21JCZDJC01100), the Beijing-Tianjin-Hebei Basic Research Cooperation Project (J230012), and Taishan Scholar Young Expert (tsqz20221168).

### Appendix A. Supplementary data

Supplementary data to this article can be found online at <https://doi.org/10.1016/j.bioactmat.2024.11.032>.

### References

- [1] S.A. Quadri, M. Farooqui, A. Ikram, A. Zafar, M.A. Khan, S.S. Suriya, C.F. Claus, B. Fiani, M. Rahman, A. Ramachandran, I.I.T. Armstrong, M.A. Taqi, M. M. Mortazavi, Recent update on basic mechanisms of spinal cord injury, *Neurosurg. Rev.* 43 (2020) 425–441, <https://doi.org/10.1007/s10143-018-1008-3>.
- [2] A. Cugurra, T. Mamuladze, J. Rustenhoven, T. Dykstra, G. Beroshvili, Z. J. Greenberg, W. Baker, Z. Papadopoulos, A. Drieu, S. Blackburn, M. Kanamori, S. Briosci, J. Herz, L.G. Schuettelpelz, M. Colonna, I. Smirnov, J. Kipnis, Skull and vertebral bone marrow are myeloid cell reservoirs for the meninges and CNS parenchyma, *Science* 373 (2021) eabf7844, <https://doi.org/10.1126/science.abf7844>.
- [3] S.M. Lee, S. Rosen, P. Weinstein, N. van Rooijen, L.J. Noble-Haeusslein, Prevention of both neutrophil and monocyte recruitment promotes recovery after spinal cord injury, *J. Neurotrauma* 28 (2011) 1893–1907, <https://doi.org/10.1089/neu.2011.1860>.
- [4] B.K. Kwon, E. Okon, J. Hillyer, C. Mann, D. Baptiste, L.C. Weaver, M.G. Fehlings, W. Tetzlaff, A systematic review of non-invasive pharmacologic neuroprotective treatments for acute spinal cord injury, *J. Neurotrauma* 28 (2011) 1545–1588, <https://doi.org/10.1089/neu.2009.1149>.
- [5] Y. Zhu, C. Soderblom, V. Krishnan, J. Ashbaugh, J.R. Bethea, J.K. Lee, Hematogenous macrophage depletion reduces the fibrotic scar and increases axonal growth after spinal cord injury, *Neurobiol. Dis.* 74 (2015) 114–125, <https://doi.org/10.1016/j.nbd.2014.10.024>.
- [6] X. Freyermuth-Trujillo, J.J. Segura-Urbe, H. Salgado-Ceballos, C.E. Orozco-Barrios, A. Coyoy-Salgado, Inflammation: a target for treatment in spinal cord injury, *Cells* 11 (2022) 2692, <https://doi.org/10.3390/cells11172692>.
- [7] L.B. Kennedy, A.K.S. Salama, A review of cancer immunotherapy toxicity, *CA Cancer J. Clin.* 70 (2020) 86–104, <https://doi.org/10.3322/caac.21596>.
- [8] J.E. Yoo, M. Kim, B. Kim, H. Lee, W.H. Chang, J. Yoo, K. Han, D.W. Shin, Increased risk of Myocardial Infarction, Heart failure, and Atrial Fibrillation after spinal cord injury, *J. Am. Coll. Cardiol.* 83 (2024) 741–751, <https://doi.org/10.1016/j.jacc.2023.12.010>.
- [9] Ł. Szymczak, T. Podgórski, K. Domaszewska, Comparison of the levels of hematological parameters at rest and after maximum exercise between physically active people with spinal cord injury and able-bodied people, *Int. J. Environ. Res. Public Health.* 18 (2021) 12323, <https://doi.org/10.3390/ijerph182312323>.
- [10] R.F. Taylor, L.P. Schramm, Differential effects of spinal transection on sympathetic nerve activities in rats, *Am. J. Physiol.* 253 (1987) R611–R618, <https://doi.org/10.1152/ajpregu.1987.253.4.r611>.
- [11] K.M. Lucin, V.M. Sanders, T.B. Jones, W.B. Malarkey, P.G. Popovich, Impaired antibody synthesis after spinal cord injury is level dependent and is due to sympathetic nervous system dysregulation, *Exp. Neurol.* 207 (2007) 75–84, <https://doi.org/10.1016/j.expneurol.2007.05.019>.
- [12] J.E. Soriano, R. Hudelle, J.W. Squair, L. Mahe, S. Amir, M. Gautier, V.P. Puchalt, Q. Barraud, A.A. Phillips, G. Courtine, Longitudinal interrogation of sympathetic neural circuits and hemodynamics in preclinical models, *Nat. Protoc.* 18 (2023) 340–373, <https://doi.org/10.1038/s41596-022-00764-w>.
- [13] M. Ueno, Y. Ueno-Nakamura, J. Niehaus, P.G. Popovich, Y. Yoshida, Silencing spinal interneurons inhibits immune suppressive autonomic reflexes caused by spinal cord injury, *Nat. Neurosci.* 19 (2016) 784–787, <https://doi.org/10.1038/nn.4289>.
- [14] Y. Zhang, Z. Guan, B. Reader, T. Shawler, S. Mandrekar-Colucci, K. Huang, Z. Weil, A. Bratasz, J. Wells, N.D. Powell, J.F. Sheridan, C.C. Whitacre, A.G. Rabchevsky, M. S. Nash, P.G. Popovich, Autonomic dysreflexia causes chronic immune suppression after spinal cord injury, *J. Neurosci.* 33 (2013) 12970–12981, <https://doi.org/10.1523/jneurosci.1974-13.2013>.
- [15] H. Prüss, A. Tedeschi, A. Thiriou, L. Lynch, S.M. Loughhead, S. Stutte, I.B. Mazo, M. A. Kopp, B. Brommer, C. Blex, L.C. Geurtz, T. Liebscher, A. Niedeggen, U. Dirnagl, F. Bradke, M.S. Volz, M.J. DeVivo, Y. Chen, U.H. von Andrian, J.M. Schwab, Spinal cord injury-induced immunodeficiency is mediated by a sympathetic-neuroendocrine adrenal reflex, *Nat. Neurosci.* 20 (2017) 1549–1559, <https://doi.org/10.1038/nn.4643>.
- [16] R.S. Carpenter, J.M. Marbourg, F.H. Brennan, K.A. Mifflin, J.C.E. Hall, R.R. Jiang, X.M. Mo, M. Karunasiri, M.H. Burke, A.M. Dorrance, P.G. Popovich, Spinal cord injury causes chronic bone marrow failure, *Nat. Commun.* 11 (2020) 3702, <https://doi.org/10.1038/s41467-020-17564-z>.
- [17] M.A. Oropallo, R. Goenka, M.P. Cancro, Spinal cord injury impacts B cell production, homeostasis, and activation, *Semin. Immunol.* 26 (2014) 421–427, <https://doi.org/10.1016/j.smim.2014.09.014>.
- [18] K.S. Held, T.E. Lane, Spinal cord injury, immunodepression, and antigenic challenge, *Semin. Immunol.* 26 (2014) 415–420, <https://doi.org/10.1016/j.smim.2014.03.003>.
- [19] B.T. Noble, F.H. Brennan, P.G. Popovich, The spleen as a neuroimmune interface after spinal cord injury, *J. Neuroimmunol.* 321 (2018) 1–11, <https://doi.org/10.1016/j.jneuroim.2018.05.007>.
- [20] R. Cao, A. Thatavarty, K.Y. King, Forged in the fire: Lasting impacts of inflammation on hematopoietic progenitors, *Exp. Hematol.* 134 (2024) 104215, <https://doi.org/10.1016/j.exphem.2024.104215>.
- [21] S.X. Shi, K. Shi, Q. Liu, Brain injury instructs bone marrow cellular lineage destination to reduce neuroinflammation, *Sci. Transl. Med.* 13 (2021), <https://doi.org/10.1126/scitranslmed.abc7029> eabc7029.
- [22] H. Cheng, Z. Zheng, T. Cheng, New paradigms on hematopoietic stem cell differentiation, *Protein Cell* 11 (2020) 34–44, <https://doi.org/10.1007/s13238-019-0633-0>.
- [23] S. Gur-Cohen, T. Itkin, S. Chakrabarty, C. Graf, O. Kollet, A. Ludin, K. Golan, A. Kalinkovich, G. Ledergor, E. Wong, E. Niemeyer, Z. Porat, A. Erez, I. Sagi, C. T. Esmon, W. Ruf, T. Lapidot, PARI signaling regulates the retention and recruitment of EPCR-expressing bone marrow hematopoietic stem cells, *Nat. Med.* 21 (2015) 1307–1317, <https://doi.org/10.1038/nm.3960>.
- [24] J. Hoggatt, P. Singh, T.A. Tate, B.K. Chou, S.R. Datari, S. Fukuda, L. Liu, P. V. Kharchenko, A. Schajnovitz, N. Baryawno, F.E. Mercier, J. Boyer, J. Gardner, D. M. Morrow, D.T. Scadden, L.M. Pelus, Rapid mobilization reveals a highly Engraftable hematopoietic stem cell, *Cell* 172 (2018) 191–204.e110, <https://doi.org/10.1016/j.cell.2017.11.003>.
- [25] T. Sugiyama, H. Kohara, M. Noda, T. Nagasawa, Maintenance of the hematopoietic stem cell pool by CXCL12-CXCR4 chemokine signaling in bone marrow stromal cell

- niches, *Immunity* 25 (2006) 977–988, <https://doi.org/10.1016/j.immuni.2006.10.016>.
- [26] T. Li, K. Zhang, R. Liu, L. Ren, X. Li, J. Li, W. Liu, Y. Song, Direct infusion-multiple reaction monitoring cubed (DI-MRM(3)) enables widely targeted bi-omics of Colla Corii Asini (Chinese name: Ejiao), *Food Chem.* 447 (2024) 138969, <https://doi.org/10.1016/j.foodchem.2024.138969>.
- [27] Y. Zhang, T. Ye, S. Gong, Z. Hong, X. Zhou, H. Liu, H. Qu, J. Qian, RNA-sequencing based bone marrow cell transcriptome analysis reveals the potential mechanisms of E'jiao against blood-deficiency in mice, *Biomed. Pharmacother.* 118 (2019) 109291, <https://doi.org/10.1016/j.biopha.2019.109291>.
- [28] Q. Yue, W. Zhang, S. Lin, T. Zheng, Y. Hou, Y. Zhang, Z. Li, K. Wang, L. Yue, B. Abay, M. Li, L. Fan, Ejiao ameliorates lipopolysaccharide-induced pulmonary inflammation via inhibition of NFκB regulating NLRP3 inflammasome and mitochondrial ROS, *Biomed. Pharmacother.* 152 (2022) 113275, <https://doi.org/10.1016/j.biopha.2022.113275>.
- [29] E.M. Pietras, D. Reynaud, Y.A. Kang, D. Carlin, F.J. Calero-Nieto, A.D. Leavitt, J. M. Stuart, B. Götgens, E. Passegué, Functionally distinct subsets of lineage-Biased multipotent progenitors control blood production in normal and regenerative conditions, *Cell Stem Cell* 17 (2015) 35–46, <https://doi.org/10.1016/j.stem.2015.05.003>.
- [30] Y. Xu, B. Wang, M. Zhang, J. Zhang, Y. Li, P. Jia, H. Zhang, L. Duan, Y. Li, Y. Li, X. Qu, S. Wang, D. Liu, W. Zhou, H. Zhao, H. Zhang, L. Chen, X. An, S. Lu, S. Zhang, Carbon dots as a potential therapeutic agent for the treatment of cancer-related anemia, *Adv. Mater.* 34 (2022) e2200905, <https://doi.org/10.1002/adma.202200905>.
- [31] P.O. Iversen, N. Hjeltne, B. Holm, T. Flatebo, I. Strom-Gundersen, W. Ronning, J. Stanghelle, H.B. Benestad, Depressed immunity and impaired proliferation of hematopoietic progenitor cells in patients with complete spinal cord injury, *Blood* 96 (2000) 2081–2083.
- [32] J. Frisbie, Anemia and hypoalbuminemia of chronic spinal cord injury: prevalence and prognostic significance, *Spinal Cord* 48 (2010) 566–569, <https://doi.org/10.1038/sc.2009.163>.
- [33] C.T. Huang, M.J. DeVivo, S.L. Stover, Anemia in acute phase of spinal cord injury, *Arch. Phys. Med. Rehabil.* 71 (1990) 3–7.
- [34] J. Carrelha, Y. Meng, L.M. Kettyle, T.C. Luis, R. Norfo, V. Alcolea, H. Boukarabila, F. Grasso, A. Gambardella, A. Grover, K. Högstrand, A.M. Lord, A. Sanjuan-Pla, P. S. Woll, C. Nerlov, S.E.W. Jacobsen, Hierarchically related lineage-restricted fates of multipotent haematopoietic stem cells, *Nature* 554 (7690) (2018 Feb 1) 106–111, <https://doi.org/10.1038/nature25455>.
- [35] L.M. Milich, C.B. Ryan, J.K. Lee, The origin, fate, and contribution of macrophages to spinal cord injury pathology, *Acta Neuropathol.* 137 (2019) 785–797, <https://doi.org/10.1007/s00401-019-01992-3>.
- [36] D.M. Norden, T.D. Faw, D.B. McKim, R.J. Deibert, L.C. Fisher, J.F. Sheridan, J. P. Godbout, D.M. Basso, Bone marrow-derived monocytes drive the inflammatory microenvironment in local and Remote regions after Thoracic spinal cord injury, *J. Neurotrauma* 36 (2019) 937–949, <https://doi.org/10.1089/neu.2018.5806>.
- [37] T. Kageoka, [Reticulocyte as indication of the erythroid hematopoiesis: reticulocyte fractions in peripheral blood and bone marrow], *Rinsho Byori* 49 (2001) 485–489.
- [38] S.H. Lee, S.J. Ho, D.T. Thomas, P. Giri, H. Lee, H. Sia, L.B. To, R.T. Sullivan, A partial nucleated differential cell count of the bone marrow aspirate that is independent of peripheral blood dilution, *Int. J. Lab. Hematol.* 30 (2008) 473–479, <https://doi.org/10.1111/j.1751-553X.2007.00980.x>.
- [39] S. Li, R. Champlin, J.H. Fitch, R.P. Gale, Abnormalities of myeloid progenitor cells after "successful" bone marrow transplantation, *J. Clin. Invest.* 75 (1985) 234–241, <https://doi.org/10.1172/jci111679>.
- [40] A. Chow, D. Lucas, A. Hidalgo, S. Méndez-Ferrer, D. Hashimoto, C. Scheiermann, M. Battista, M. Leboeuf, C. Prophete, N. van Rooijen, M. Tanaka, M. Merad, P. S. Frenette, Bone marrow CD169+ macrophages promote the retention of hematopoietic stem and progenitor cells in the mesenchymal stem cell niche, *J. Exp. Med.* 208 (2011) 261–271, <https://doi.org/10.1084/jem.20101688>.
- [41] Y. Luo, L. Shao, J. Chang, W. Feng, Y.L. Liu, M.H. Cottler-Fox, P.D. Emanuel, M. Hauer-Jensen, I.D. Bernstein, L. Liu, X. Chen, J. Zhou, P.J. Murray, D. Zhou, M1 and M2 macrophages differentially regulate hematopoietic stem cell self-renewal and ex vivo expansion, *Blood Adv* 2 (2018) 859–870, <https://doi.org/10.1182/bloodadvances.2018015685>.
- [42] H. Chen, C. Xu, H. Zeng, Z. Zhang, N. Wang, Y. Guo, Y. Zheng, S. Xia, H. Zhou, X. Yu, X. Fu, T. Tang, X. Wu, Z. Chen, Y. Peng, J. Cai, J. Li, F. Yan, C. Gu, G. Chen, J. Chen, Ly6C-high monocytes alleviate brain injury in experimental subarachnoid hemorrhage in mice, *J. Neuroinflammation* 20 (2023) 270, <https://doi.org/10.1186/s12974-023-02939-y>.
- [43] L.V. Blomster, F.H. Brennan, H.W. Lao, D.W. Harle, A.R. Harvey, M.J. Ruitenberg, Mobilisation of the splenic monocyte reservoir and peripheral CX3CR1 deficiency adversely affects recovery from spinal cord injury, *Exp. Neurol.* 247 (2013) 226–240, <https://doi.org/10.1016/j.expneurol.2013.05.002>.
- [44] D.J. Hellenbrand, C.M. Quinn, Z.J. Piper, C.N. Morehouse, J.A. Fixel, A.S. Hanna, Inflammation after spinal cord injury: a review of the critical timeline of signaling cues and cellular infiltration, *J. Neuroinflammation* 18 (2021) 284, <https://doi.org/10.1186/s12974-021-02337-2>.
- [45] T. Röszer, Understanding the Mysterious M2 macrophage through activation markers and effector mechanisms, *Mediators Inflamm* 2015 (2015) 816460, <https://doi.org/10.1155/2015/816460>.
- [46] S. Monteiro, A.G. Pinho, M. Macieira, C. Serre-Miranda, J.R. Cibrão, R. Lima, C. Soares-Cunha, N.L. Vasconcelos, J. Lentilhas-Graça, S. Duarte-Silva, A. Miranda, M. Correia-Neves, A.J. Salgado, N.A. Silva, Splenic sympathetic signaling contributes to acute neutrophil infiltration of the injured spinal cord, *J. Neuroinflammation* 17 (2020) 282, <https://doi.org/10.1186/s12974-020-01945-8>.
- [47] F.K. Swirski, M. Nahrendorf, M. Etzrodt, M. Wildgruber, V. Cortez-Retamozo, P. Panizzi, J.L. Figueiredo, R.H. Kohler, A. Chudnovskiy, P. Waterman, E. Aikawa, T.R. Mempel, P. Libby, R. Weissleder, M.J. Pittet, Identification of splenic reservoir monocytes and their deployment to inflammatory sites, *Science* 325 (2009) 612–616, <https://doi.org/10.1126/science.1175202>.
- [48] K.M. Lucin, V.M. Sanders, T.B. Jones, W.B. Malarkey, P.G. Popovich, Impaired antibody synthesis after spinal cord injury is level dependent and is due to sympathetic nervous system dysregulation, *Exp. Neurol.* 207 (2007) 75–84, <https://doi.org/10.1016/j.expneurol.2007.05.019>.
- [49] V. Cortez-Retamozo, M. Etzrodt, A. Newton, R. Ryan, F. Pucci, S.W. Sio, W. Kuswanto, P.J. Rauch, A. Chudnovskiy, Y. Iwamoto, R. Kohler, B. Marinelli, R. Gorbato, G. Wojtkiewicz, P. Panizzi, M. Mino-Kenudson, R. Forghani, J. L. Figueiredo, J.W. Chen, R. Xavier, F.K. Swirski, M. Nahrendorf, R. Weissleder, M. J. Pittet, Angiotensin II drives the production of tumor-promoting macrophages, *Immunity* 38 (2013) 296–308, <https://doi.org/10.1016/j.immuni.2012.10.015>.
- [50] M. Maryanovich, S. Takeishi, P.S. Frenette, Neural regulation of bone and bone marrow, *Cold Spring Harb. Perspect. Med.* 8 (2018) a031344, <https://doi.org/10.1101/cshperspect.a031344>.
- [51] H.J. Junge, S. Yang, J.B. Burton, K. Paes, X. Shu, D.M. French, M. Costa, D.S. Rice, W. Ye, TSPAN12 regulates retinal vascular development by promoting Norrin- but not Wnt-induced FZD4/beta-catenin signaling, *Cell* 139 (2009) 299–311, <https://doi.org/10.1016/j.cell.2009.07.048>.
- [52] W. Skronska-Wasek, K. Mutze, H.A. Baarsma, K.R. Bracke, H.N. Alsafadi, M. Lehmann, R. Costa, M. Stornaiuolo, E. Novellino, G.G. Brusselle, D.E. Wagner, A.Ö. Yildirim, M. Königshoff, Reduced Frizzled receptor 4 expression Prevents WNT/β-Catenin-driven Alveolar lung repair in chronic Obstructive pulmonary disease, *Am. J. Respir. Crit. Care Med.* 196 (2017) 172–185, <https://doi.org/10.1164/rccm.201605-0904OC>.
- [53] L. Tickenbrock, J. Schwäble, M. Wiedehage, B. Steffen, B. Sargin, C. Choudhary, C. Brandts, W.E. Berdel, C. Müller-Tidow, H. Serve, Fli3 tandem duplication mutations cooperate with Wnt signaling in leukemic signal transduction, *Blood* 105 (2005) 3699–3706, <https://doi.org/10.1182/blood-2004-07-2924>.
- [54] P.M. Corrigan, E. Dobbin, R.W. Freeburn, H. Wheadon, Patterns of Wnt/Fzd/LRP gene expression during embryonic hematopoiesis, *Stem Cells Dev* 18 (2009) 759–772, <https://doi.org/10.1089/scd.2008.0270>.
- [55] C.J. Cain, J.O. Manilay, Hematopoietic stem cell fate decisions are regulated by Wnt antagonists: comparisons and current controversies, *Exp. Hematol.* 41 (2013) 3–16, <https://doi.org/10.1016/j.exphem.2012.09.006>.
- [56] L. Tickenbrock, S. Hehn, B. Sargin, C. Choudhary, N. Bäumer, H. Buerger, B. Schulte, A. Müller, W.E. Berdel, C. Müller-Tidow, H. Serve, Activation of Wnt signalling in acute myeloid leukemia by induction of Frizzled-4, *Int. J. Oncol.* 33 (2008) 1215–1221.
- [57] N. Cabezas-Wallscheid, D. Klimmeck, J. Hansson, D.B. Lipka, A. Reyes, Q. Wang, D. Weichenhan, A. Lier, L. von Paleske, S. Renders, P. Wünsche, P. Zeisberger, D. Brocks, L. Gu, C. Herrmann, S. Haas, M.A.G. Essers, B. Brors, R. Eils, W. Huber, M.D. Milsom, C. Plass, J. Krijgsvelde, A. Trumpp, Identification of regulatory networks in HSCs and their immediate progeny via Integrated Proteome, transcriptome, and DNA Methylation analysis, *Cell Stem Cell* 15 (2014) 507–522, <https://doi.org/10.1016/j.stem.2014.07.005>.
- [58] T. Yuan, W. Liu, T. Wang, F. Ye, J. Zhang, Z. Gu, J. Xu, Y. Li, Natural Polyphenol delivered methylprednisolone achieve targeted enrichment for acute spinal cord injury therapy, *Small* (2024) e2404815, <https://doi.org/10.1002/sml.202404815>.
- [59] G. Zheng, W. Yu, Z. Xu, C. Yang, Y. Wang, Z. Yue, Q. Xiao, W. Zhang, X. Wu, F. Zang, J. Wang, L. Wang, W.E. Yuan, B. Hu, H. Chen, Neuroimmune modulating and energy supporting nanzyme-mimic scaffold synergistically promotes axon regeneration after spinal cord injury, *J. Nanobiotechnology.* 22 (2024) 399, <https://doi.org/10.1186/s12951-024-02594-2>.
- [60] G. Yuan, Z. Li, X. Lin, N. Li, R. Xu, New perspective of skeletal stem cells, *Biomater. Transl.* 3 (2022) 280–294, <https://doi.org/10.12336/biomatertransl.2022.04.007>.
- [61] Y. Li, A.M. Lucas-Osma, S. Black, M.V. Bandet, M.J. Stephens, R. Vavrek, L. Sanelli, K.K. Fenrich, A.F. Di Narzo, S. Dracheva, I.R. Winship, K. Fouad, D.J. Bennett, Pericytes impair capillary blood flow and motor function after chronic spinal cord injury, *Nat. Med.* 23 (2017) 733–741, <https://doi.org/10.1038/nm.4331>.
- [62] H.S. Chhabra, K. Sarda, Clinical translation of stem cell based interventions for spinal cord injury - are we there yet? *Adv. Drug Deliv. Rev.* 120 (2017) 41–49, <https://doi.org/10.1016/j.addr.2017.09.021>.
- [63] Z. Liu, Y. Yang, L. He, M. Pang, C. Luo, B. Liu, L. Rong, High-dose methylprednisolone for acute traumatic spinal cord injury: a meta-analysis, *Neurology* 93 (2019) e841–e850, <https://doi.org/10.1212/wnl.0000000000007998>.
- [64] N. Ding, F. Zhou, G. Li, H. Shen, L. Bai, J. Su, Quantum dots for bone tissue engineering, *Mater. Today Bio.* 28 (2024) 101167, <https://doi.org/10.1016/j.mtbio.2024.101167>.
- [65] M. Li, B. Yu, S. Wang, F. Zhou, J. Cui, J. Su, Microenvironment-responsive nanocarriers for targeted bone disease therapy, *Nano Today* 50 (2023) 101838, <https://doi.org/10.1016/j.nantod.2023.101838>.
- [66] A. Truskewycz, H. Yin, N. Halberg, D.T.H. Lai, A.S. Ball, V.K. Truong, A. M. Rybicka, I. Cole, Carbon dot therapeutic platforms: administration, distribution, metabolism, excretion, toxicity, and therapeutic potential, *Small* 18 (2022) 2106342, <https://doi.org/10.1002/sml.202106342>.
- [67] A.T. Krasley, E. Li, J.M. Galeana, C. Bulumulla, A.G. Beyene, G.S. Demirer, Carbon nanomaterial fluorescent probes and their biological applications, *Chem. Rev.* 124 (2024) 3085–3185, <https://doi.org/10.1021/acs.chemrev.3c00581>.

- [68] L. Đorđević, F. Arcudi, M. Cacioppo, M.A. Prato, Multifunctional chemical toolbox to engineer carbon dots for biomedical and energy applications, *Nat. Nanotechnol.* 17 (2022) 112–130, <https://doi.org/10.1038/s41565-021-01051-7>.
- [69] B. Wang, S. Lu, The light of carbon dots: from mechanism to applications, *Matter* 5 (2022) 110–149.
- [70] Y. Zhang, T. Ye, Z. Hong, S. Gong, X. Zhou, H. Liu, J. Qian, H. Qu, Pharmacological and transcriptome profiling analyses of Fufang E'jiao Jiang during chemotherapy-induced myelosuppression in mice, *J. Ethnopharmacol.* 238 (2019) 111869, <https://doi.org/10.1016/j.jep.2019.111869>.
- [71] X. Li, Y. Zhang, Z. Hong, S. Gong, W. Liu, X. Zhou, Y. Sun, J. Qian J, H. Qu, Transcriptome profiling analysis reveals the potential mechanisms of three Bioactive Ingredients of Fufang E'jiao Jiang during chemotherapy-induced myelosuppression in mice, *Front. Pharmacol.* 9 (2018 Jun 13) 616, <https://doi.org/10.3389/fphar.2018.00616>.
- [72] M. Liu, H. Tan, X. Zhang, Z. Liu, Y. Cheng, D. Wang, F. Wang, Hematopoietic effects and mechanisms of Fufang E' jiao Jiang on radiotherapy and chemotherapy-induced myelosuppressed mice, *J. Ethnopharmacol.* 152 (2014) 575–584, <https://doi.org/10.1016/j.jep.2014.02.012>.
- [73] X. Zhang, M. Chang, B. Wang, X. Liu, Z. Zhang, G. Han, YAP/WNT5A/FZD4 axis regulates osteogenic differentiation of human periodontal ligament cells under cyclic stretch, *J. Periodontol. Res.* 58 (2023) 907–918, <https://doi.org/10.1111/jre.13143>.
- [74] J. Ding, S.J. Lee, L. Vlahos, K. Yuki, C.C. Rada, V. van Unen, M. Vuppapalaty, H. Chen, A. Sura, A.K. McCormick, M. Tomaske, S. Alwahabi, H. Nguyen, W. Nowatzke, L. Kim, L. Kelly, D. Vollrath, A. Califano, W.C. Yeh, Y. Li, C.J. Kuo, Therapeutic blood-brain barrier modulation and stroke treatment by a bioengineered FZD(4)-selective WNT surrogate in mice, *Nat. Commun.* 14 (2023) 2947, <https://doi.org/10.1038/s41467-023-37689-1>.